The organizer of chromatin topology RIF1 ensures cellular resilience to DNA replication stress.

Cyril Ribeyre[1], Rana Lebdy[1,3], Julie Patouillard[1], Marion Larroque[2], Raghida Abou-Merhi[3], Christian Larroque[4] and Angelos Constantinou[1].

[1]Institut de Génétique Humaine (UMR9002), Centre National de la Recherche Scientifique, Université de Montpellier.
141, Rue de la Cardonille, 34396 Montpellier Cedex 5, France

[2]Institut du Cancer de Montpellier, Montpellier, France
208, Avenue des Apothicaires, 34298 Montpellier Cedex 5, France

[3]Doctoral School of Sciences and Technology-DSST
Rafic Hariri Campus, Lebanese University, Hadath, Lebanon

[4]Institut de Recherche en Cancérologie de Montpellier (U1194), Université de Montpellier, Institut National de la Santé et de la Recherche Médicale
208, avenue des Apothicaires, 34298 Montpellier Cedex 5, France

Correspondence: cyril.ribeyre@igh.cnrs.fr or angelos.constantinou@igh.cnrs.fr

Running title: RIF1 stabilizes replication domains.

Abstract

Eukaryotic genomes are duplicated from thousands of replication origins that fire sequentially forming a defined spatiotemporal pattern of replication clusters. The temporal order of DNA replication is determined by chromatin architecture and, more specifically, by chromatin contacts that are stabilized by RIF1. Here we show that RIF1 localizes in close proximity to newly synthesized DNA. In cells exposed to the DNA replication inhibitor aphidicolin, suppression of RIF1 markedly decreased the efficacy of protein isolation on nascent DNA (iPOND), suggesting that the iPOND procedure is biased by chromatin topology. RIF1 was required to limit the accumulation of DNA lesions induced by aphidicolin treatment and promoted the recruitment of cohesins in the vicinity of nascent DNA. Collectively, the data suggest that the stabilization of chromatin topology by RIF1 limits replication-associated genomic instability.

Keywords: RIF1/replicative stress/nuclear topology/iPOND/cohesin

38 **Introduction**

39 The duplication of a complete genome is a formidable task that must be perfectly controlled to avoid
40 the transmission of mutations or chromosomal rearrangements to daughter cells. Two meters of DNA
41 are packed and replicated in a human cell of about 10 μm of diameter. Hence, the spatiotemporal
42 program of DNA replication is largely defined by the global organization of the nucleus (Marchal et al.,
43 2019). DNA replication is initiated from defined regions of the genome called origins of replication.
44 More than 30000 replication origins are required for the duplication of the human genome (Mechali,
45 2010). When replication forks stall, the firing of backup origins (also known as dormant origins) ensure
46 the completion of DNA replication (Blow et al., 2011). The timing of replication is influenced by the 3D
47 organization of chromatin architecture (Courbet et al., 2008; Foti et al., 2016; Klein et al., 2021).
48 Cohesins influence origins firing locally (Guillou et al., 2010), yet without determining replication timing
49 globally (Oldach and Nieduszynski, 2019), most likely via the formation of loops by extrusion (Davidson
50 et al., 2019; Kim et al., 2019). RIF1, a conserved protein involved in telomeres capping, DNA double-
51 strand break repair and chromatin organization, controls the timing of DNA replication (Cornacchia et
52 al., 2012; Foti et al., 2016; Hayano et al., 2012; Klein et al., 2021; Mattarocci et al., 2016; Yamazaki et
53 al., 2012). RIF1 determines replication timing via the stabilization of chromatin architecture (Foti et al.,
54 2016; Kanoh et al., 2015; Klein et al., 2021; Yamazaki et al., 2013), and may regulate origin licensing
55 owing to its interaction with PP1 phosphatase that would counteract DDK kinases (Dave et al., 2014;
56 Hiraga et al., 2014; Mattarocci et al., 2014).

57 Throughout S phase, different nuclear patterns of replication foci reflect the orderly and sequential
58 replication of chromatin domains (Chagin et al., 2016; Dimitrova and Berezney, 2002). Replication forks
59 encounter a variety of impediments from both endogenous and exogenous sources (Lambert and Carr,
60 2013; Zeman and Cimprich, 2014). The slowing or stalling of replication forks by these impediments
61 induces the activation of the checkpoint kinase ATR, which ensures that DNA synthesis within actively
62 replicating chromosomal domains is completed before the duplication of a new chromosomal domain
63 has started. ATR signaling delays the activation of late replication domains while promoting the firing
64 of dormant origins within active replication domains (Blow et al., 2011). This suggests that the nuclear
65 architecture contributes to cellular resilience to DNA replication stress. In support of this, Lamin A/C is
66 required for the maintenance of chromosome integrity when the progression of replication forks is
67 impeded by DNA lesions or upon nucleotide depletion (Singh et al., 2013). Furthermore, the
68 association of Lamin A/C with the DNA polymerase clamp PCNA is critical for replication forks stability
69 (Cobb et al., 2016). Hutchinson-Gilford progeria syndrome is caused by a mutation of the LMNA gene
70 that leads to an aberrant Lamin A protein named progerin. The association of progerin with PCNA alters
71 the nuclear distribution of PCNA, induces ATR activation and the formation of γH2A.X (Wheaton et al.,

2017). In budding yeast, cohesins accumulate in the vicinity of replication forks upon treatment with hydroxyurea and are required for replication fork restart (Tittel-Elmer et al., 2012). These examples illustrate the links between replicative stress and nuclear structures, which remain incompletely understood.

The isolation of Proteins on Nascent DNA coupled with Mass Spectrometry (iPOND-MS) allows the identification of proteins localized in the vicinity of active replication forks (Aranda et al., 2014; Dungrawala et al., 2015; Lopez-Contreras et al., 2013; Lossaint et al., 2013; Sirbu et al., 2011; Sirbu et al., 2013). iPOND experiments performed under various experimental conditions have revealed components of the replication machinery (e.g. PCNA and DNA polymerases), proteins that accumulate near forks under stressful conditions (e.g. ATR and FANCD2), proteins that are required for the restoration of chromatin structures after passage of the replication fork (e.g. histones) and proteins that are playing a structural roles such as Lamin A (Alabert et al., 2014; Dungrawala et al., 2015; Lopez-Contreras et al., 2013; Lossaint et al., 2013; Ribeyre et al., 2016; Sirbu et al., 2011; Sirbu et al., 2013; Wheaton et al., 2017).

Here we provide evidence that during S phase, RIF1 is proximal to newly synthesized DNA. In cells exposed to the DNA polymerase inhibitor aphidicolin, RIF1 promotes the recruitment of the cohesin subunits SMC1 and SMC3 near replication forks and stabilizes replicating nucleoprotein clusters isolated by iPOND. We propose that the stabilization of chromatin architecture by RIF1 and cohesin limits the formation of DNA lesions caused by DNA replication impediments.

94 **Results**

95 **iPOND coupled with mass spectrometry identifies proteins involved in nuclear organization.**

96 To identify new proteins in vicinity of replication forks we performed iPOND-MS using a highly sensitive
97 last generation mass spectrometer (Sciex TripleTOF 5600+) and quantified the results using MaxQuant
98 (Cox and Mann, 2008). We analyzed the data using Perseus (Tyanova et al., 2016) and took advantage
99 of a volcano plot representation to visualize the proteins significantly enriched upon EdU pulse
100 compared to a 2 hours thymidine chase (Figure 1A). As expected, most of the known proteins of the
101 replisome (e.g., PCNA, RFC subunits, MCM1-6, FEN1 or DNA polymerases) were clearly enriched. We
102 identified also a large number of proteins that were not previously described as replisome components
103 that will be analyzed elsewhere. Interestingly, the iPOND-MS data revealed an enrichment of several
104 cohesin subunits (SMC3, SMC1A, STAG2, RAD21, PDS5A and PDS5B) near forks (Figure 1A). Since
105 cohesins are thought to play an architectural role at replication foci (Guillou et al., 2010), it is likely
106 that they are not associated directly with individual replication forks but rather with chromatin domain
107 undergoing replication. In contrast, Lamin B1 and Lamin B2 were not enriched after EdU pulse (Figure
108 1A), indicating that not all the structural components of the nucleus are localized in proximity of active
109 replisomes. Interestingly, we identified RIF1 as a protein associated with nascent DNA (Figure 1A),
110 consistent with previous studies (Alabert et al., 2014; Munden et al., 2018). We confirmed this data
111 using an antibody directed against RIF1 (Figure 1B). This indicates that RIF1 localizes in the vicinity of
112 active replication forks. Consistent with this, we detected RIF1 in immune-precipitates of the
113 endogenous DNA polymerase clamp PCNA (Figure 1C).

114 **RIF1 protects the integrity of replication forks upon prolonged replicative stress.**

115 Although RIF1 located near active replisomes, suppression of RIF1 did not alter significantly the
116 progression of replication forks (SupFig1A), consistent with previous studies (Cornacchia et al., 2012;
117 Ray Chaudhuri et al., 2016). A higher frequency of stalled forks, however, is observed in *rif1*$^{-/-}$ DT40
118 cells (Xu et al., 2010), suggesting that RIF1 could be important for fork progression in some contexts.
119 Consistent with this, several studies have detected the activation of the checkpoint effector kinase
120 Chk1 in RIF1-depleted cells (Chapman et al., 2013; Foti et al., 2016). We confirmed that Chk1 was active
121 by phosphorylation on Serine 345 upon suppression of RIF1 by means of siRNAs (SupFig1B). We
122 observed also that RPA32 was phosphorylated on Ser4/8, suggesting that RIF1 depleted cells
123 accumulate DNA lesions (SupFig1B). Interestingly, RIF1 recruitment at replication forks is slightly
124 increased upon hydroxyurea (HU) treatment to limit DNA2-mediated DNA resection and DNA lesions
125 (Garzón et al., 2019; Mukherjee et al., 2019; Ray Chaudhuri et al., 2016). Consistent with this, DNA
126 lesions, genetic instability and HU sensitivity are increased upon RIF1 impairment (Buonomo et al.,

127 2009; Mukherjee et al., 2019; Xu et al., 2010). This raises the possibility that the stabilization of
128 chromatin topology by RIF1 limits replication-associated DNA lesions under stressful conditions. To
129 test this, we analyzed if RIF1 loss had any impact on replication fork dynamics in the presence of
130 aphidicolin (APH). We labelled cells for 30 minutes with IdU and then for 30 minutes with CldU in
131 presence of a low dose (0.05 μM) of APH. As expected, the ratio of the lengths of CldU versus IdU tracts
132 was close to 1 in control conditions and reduced by half in presence of APH (Figure 1D, SupFig1C). The
133 status of RIF1 did not change the ratios of CldU/IdU tracts (Figure 1D, SupFig1C) indicating that RIF1
134 depletion does not play any major role in early responses to APH. As RIF1 is protecting HU-stalled forks
135 from nucleases degradation (Garzón et al., 2019; Mukherjee et al., 2019), we tested if this was also the
136 case when replication forks were blocked with APH. To do so, we treated cells 6 hours with a high dose
137 (1 μM) of APH after 30 min sequential labelling of IdU and CldU and measured the ratio between the
138 lengths of CldU and IdU tracts. The ratio was close to 1 in cells treated with a control siRNA, and below
139 1 in RIF1 depleted cells, confirming that RIF1 is indeed protecting APH-stalled forks (Figure 1E).
140 Consistent with this, prolonged treatment (24 hours) with APH, increased the percentage of γ-H2A.X-
141 positive cells to almost 2-fold (Figure 1E) and decreased by two-fold the ability of replication forks to
142 restart (SupFig1D). Altogether, these data indicate that RIF1 limits the formation of DNA lesions under
143 stressful conditions.

144 **RIF1-dependent loss of replication organization induces DNA lesions**

145 Despite its role in protection of stalled replication forks (see above), RIF1 recruitment at forks does not
146 increase significantly in response to HU (Mukherjee et al., 2019) compared to proteins such as ATR, 9-
147 1-1, TopBP1 or FANCD2/FANCI (Dungrawala et al., 2015; Lossaint et al., 2013). Therefore, we
148 hypothesize that the impact of RIF1 on nascent DNA protection may not reflect a direct role at stalled
149 replication forks. This is supported by several articles showing that RIF1 is crucial for the organization
150 of higher-order chromatin domains and for the establishment of the replication timing program (Foti
151 et al., 2016; Klein et al., 2021; Moriyama et al., 2018; Yamazaki et al., 2012). Remarkably, the mid-S
152 pattern is selectively loss upon RIF1 impairment (Yamazaki et al., 2012), this effect was attributed to
153 the impact of RIF1 in replication timing. However, we noticed that these experiments have been
154 performed in cells synchronized with thymidine block and released into S-phase. It is well established
155 that synchronization with thymidine block perturbs the pool of nucleotides and induces DNA damage
156 (Kurose et al., 2006). Thus, we hypothesized that the absence of mid-S pattern in RIF1-depleted cells
157 synchronized using a thymidine block could reflect a defect in the maintenance of chromatin topology
158 during DNA replicative stress. To test this, we compared the frequency of each pattern in asynchronous
159 conditions and in cells synchronized with thymidine block and released into S-phase upon RIF1
160 depletion (Figure 1A). In synchronous condition, we were able to reproduce the results of Yamazaki et

161 al. and observed the disappearance of the mid-S pattern upon RIF1 depletion (Figure 2B, 2C).
162 Surprisingly, in asynchronous conditions, we found that RIF1 depletion did not alter the occurrence of
163 the mid-S pattern (Figure 2B, 2C). Importantly, and as already observed (Yamazaki et al., 2012), cell-
164 cycle distribution was not significantly affected in absence of RIF1 in synchronous or asynchronous
165 conditions (SupFig2A). This result suggests that the disappearance of the mid-S pattern in RIF1
166 depleted cells is a consequence of the synchronization procedure. This observation cannot be solely
167 explained by the difference in replication timing since it should be also observed in asynchronous cells.
168 To test if synchronization procedure increases the level or replicative stress, we analyzed the level of
169 the marker of DNA damage γ-H2A.X. In an asynchronous population of cells, the depletion of RIF1 had
170 no impact on the percentage of γ-H2A.X positive cells (Figure 2B, 2D). As expected, the percentage of
171 γ-H2A.X positive cells increased 2 hours after release from the thymidine block. Strikingly, inactivation
172 of RIF1 tripled the percentage of γ-H2A.X positive cells in the same conditions (6.9% in control versus
173 24.1% in shRIF1 (1) and 19.1% in shRIF1 (2)). We conclude that the disappearance of the mid-S pattern
174 upon RIF1 depletion correlates with the formation of DNA lesions. The thymidine block procedure is
175 affecting the pool of dNTPs and therefore should have a direct impact on the progression of replication
176 forks that might be exacerbated in the absence of RIF1. To test this, we monitored the phosphorylation
177 of Chk1 on Serine 345. In control condition, we observed a mild phosphorylation of Chk1 on Serine
178 345, in line with the higher level of γ-H2A.X (Figure 2E). Interestingly, we observed a strong level of
179 Chk1 phosphorylation in RIF1-depleted cells 2 hours after release from the thymidine block (Figure 2E).
180 In asynchronous conditions, suppression of RIF1 did not significantly alter the progression of
181 replication forks (SupFig1A). Two hours after release from a thymidine block, however, replication
182 tracts were longer in the absence of RIF1 (Figure 2F, SupFig2B). Unrestrained DNA synthesis would
183 yield single-stranded DNA gaps detected and signaled by ATR, consistent with higher level of Chk1 and
184 H2A.X phosphorylation. We propose that the occurrence of DNA lesions during prolonged replicative
185 stress observed in RIF1 depleted cells is a consequence of alterations in the organization of replicated
186 chromatin domains.

187 **RIF1 impairment reduces iPOND efficiency in presence of replicative stress.**

188 We showed that prolonged treatment with APH or thymidine yields high level of γH2A.X in RIF1-
189 depleted cells. Importantly, after a thymidine block, the increase of γH2A.X signal correlates with
190 alterations of DNA replication patterns. Since APH has also been widely used for cell synchronization,
191 it is highly probable that the increase level of DNA lesions is absence of RIF1 in APH treated cells is also
192 due to a defect in the maintenance of chromatin topology. Alternatively, the data could reflect a role
193 for RIF1 in G1 cells rather than in S phase. To understand this in more details, we performed a series
194 of experiments in RIF1-depleted cells using short treatments with aphidicolin (Figure 3A). First, we

195 performed iPOND assay and probed isolated proteins by western-blotting (Figure 3B). Under standard
196 cell culture conditions, the efficacy of PCNA isolation with nascent DNA in RIF1-depleted cells was
197 similar to that of control cells (Figure 3B). As expected, a 30 min treatment with a low dose of APH (0.1
198 μM) induced the recruitment of BRCA1 and TopBP1 on nascent DNA (Figure 3B). Strikingly, in RIF1-
199 depleted cells treated with APH, the efficacy of PCNA recovery (as well as BRCA1 and TopBP1) with
200 nascent DNA diminished dramatically (Figure 3B), an observation we could reproduce with PCNA and
201 other replisomes components (SupFig3A). This observation could be the consequence of a massive
202 decrease in EdU incorporation that would impair proteins recovery. To test this hypothesis, we
203 measured EdU incorporation using immunofluorescence. As expected APH treatment reduces strongly
204 EdU incorporation but this effect was similar in RIF1-depleted cells, suggesting that EdU incorporation
205 is not impaired (Figure 3C). In addition, and consistent with Figure 1D, DNA fibers experiment
206 performed in the exact same cell line than the one used for iPOND indicate that DNA synthesis is
207 occurring, although at lower pace, in response of APH independently of the presence of RIF1 (Figure
208 3D). Thus, a defect in DNA synthesis does not account for the reduced isolation of EdU-bound proteins
209 from RIF1-depleted cells. Furthermore, we detected similar levels of the replisome-associated proteins
210 MSH2 and MCM7 in PCNA immune-precipitates from control and RIF1-depleted cells (SupFig3B),
211 suggesting that RIF1 is not required for replisome stability and replication fork progression. As this
212 step, the most reasonable hypothesis is that in presence of replicative stress, suppression of RIF1
213 reduces the efficacy of capture of EdU-associated proteins. To generalize this observation, we
214 performed the exact same iPOND experiment than in Figure 3B but analyzed the pulldowns using mass
215 spectrometry (Figure 3E). In comparison with control cells, the treatment of RIF1-depleted cell with
216 APH markedly reduced the abundance of the replication factors PCNA, MSH6, DPOD1, FEN1 and RFC4
217 captured by iPOND (Figure 3E). By contrast, changes in the efficacy of streptavidin pulldowns were not
218 observed for mitochondrial proteins such as NDUS1, NDUS3, P5CR2 and SDHA, which are also isolated
219 by iPOND (SupFig3C). To generalize this observation to the whole replisome, we summed the peptides
220 intensities of all replisome proteins listed in a previous study (Lopez-Contreras et al., 2013). In control
221 cells (shLUC), APH treatment moderately affected the recovery of replisome components (SupFig3D).
222 By contrast, APH had a severe impact on the recovery of replisome components from RIF1-depleted
223 cells (~50% decrease for shRIF1 (1) and ~33% decrease for shRIF1 (2)). The data indicate that APH
224 treatment reduces the probability to capture proteins associated with EdU-labelled DNA in RIF1-
225 depleted cells.

226 **The efficacy of iPOND is biased by chromatin topology.**

227

228 How can we explain that in cells exposed to aphidicolin, RIF1 depletion decreases the efficacy of iPOND
229 without affecting EdU incorporation? To answer to this question, one has to take into consideration
230 that the association of proteins such as cohesins or RIF1 with EdU may be indirect and determined by
231 chromatin topology. Consistent with this, methods that are using formaldehyde crosslinking such as
232 ChIP or chromosome conformation capture are indeed dependent on nuclear organization. To test if
233 iPOND efficiency is biased by chromatin organization, we took advantage of the distinct and
234 characteristic patterns formed by replicons labelled with EdU (Dimitrova and Berezney, 2002). In early
235 S-phase (replication of euchromatin), the EdU pattern is poorly clustered. Clusterization then increases
236 in mid-S phase (replication of facultative heterochromatin) and is even stronger in late S-phase
237 (replication of constitutive heterochromatin). We synchronized HeLa S3 cells using a simple thymidine
238 block procedure and released the cells in fresh media without thymidine (Figure 4A). We added EdU
239 for 15 minutes just before release (T0) and then 2 hours (T2), 4 hours (T4) and 8 hours (T8) after release
240 (Figure 4A). We verified the synchronization procedure by flow cytometry using double labelling with
241 EdU and propidium iodide (Figure 4B). As expected at T0 the majority (~80%) of the cells were in G1.
242 Two and four hours after release (T2 and T4) most of the cells (~80%) were in S-phase. After 8 hours
243 (T8), cells entered G2 and the number of S-phase cells decreased (~25%). We then performed iPOND
244 experiment on synchronized and non-synchronized cells. At T0, the PCNA signal was barely detectable,
245 as expected, and comparable to the control (minus click) of the asynchronous conditions (Figure 4C).
246 By contrast, we could observe a clear PCNA signal after the EdU-Biotin click reaction in non-
247 synchronized condition. At T2 and T4 the PCNA signal became detectable. Surprisingly the strongest
248 signal was observed at T8 despite the fact that the number of cells in S-phase is lower than in T4 and
249 T2 (Figure 4C). This observation is also true for MCM7 and H3 (Figure 4C) and is reproducible (Figure
250 4D). This result indicates that the efficacy of protein isolation on nascent DNA does not correlate
251 directly with the number of cells in S-phase. Therefore, we propose that the recovery of replisomes
252 components by iPOND is strongly dependent on the organization of replicated chromatin domains (Sup
253 Fig4). Thus, we suggest that the reduced efficacy of EdU-biotin streptavidin pulldowns in the iPOND
254 procedure and the accumulation of markers of DNA damage in RIF1 depleted cells exposed to
255 aphidicolin reflects a role for RIF1 in the stabilization of chromatin topology under DNA replication
256 stress conditions.

257 **RIF1 depletion impairs the loading of SMC1 and SMC3 at forks in presence of replicative stress**

258 RIF1 stabilizes chromatin topology via its intrinsic capacity to bridge molecules (Mattarocci et al., 2017)
259 and may promote the recruitment of additional proteins involved in the organization of chromatin
260 topology such as the cohesin complex. Indeed, cohesin are associated with replication forks in basal
261 conditions (Figure 1A) and in response to replicative stress (Ribeyre et al., 2016; Tittel-Elmer et al.,

262 2012). In addition, cohesins cooperate with RIF1 in the stabilization of chromatin topology at sites of
263 DNA double-strand breaks (Ochs et al., 2019), and organize DNA repair foci via a mechanism of loop
264 extrusion at both sites of the DNA breaks (Arnould et al., 2021). Since RIF1 depletion diminishes the
265 efficacy of the iPOND procedure, we used, as an alternative method, a proximity ligation assay (PLA,
266 Figure 5A) to analyze the loading of cohesins subunits in the vicinity of nascent DNA (Petruk et al.,
267 2017; Petruk et al., 2012; Roy et al., 2018). We first validated the method using PCNA as positive
268 control. As expected, we detected PCNA-EdU proximity signals in cells after the coupling of EdU and
269 biotin, specifically (SupFig5A). We then analyzed the recruitment of SMC1 to nascent DNA in presence
270 of 0.1μM APH. In control conditions, we observed a clear PLA signal between EdU and SMC1 confirming
271 that SMC1 is recruited near stalled replication forks (Figure 5B). Interestingly, the signal of proximity
272 between EdU and SMC1 was reduced in RIF1-depleted cells (Figure 5B, 5C, SupFig 5B). Consistent with
273 this, the localization of SMC3 to stalled forks was also dependent on RIF1 (SupFig5C). By contrast, RIF1
274 suppression had no impact on EdU-PCNA proximity signal (Figure 5B, 5C, SupFig 5B). We verified that
275 the suppression of RIF1 did not reduce the level of SMC3 and SMC1 expression (SupFig5D). Thus, we
276 conclude that RIF1 contributes to the loading of the cohesins subunits SMC1 and SMC3 near stalled
277 DNA replication forks.

278

279 **Discussion**

280 RIF1 was originally discovered more than 25 years ago in budding yeast as a negative regulator of
281 telomere elongation (Hardy et al., 1992). It is now clearly established that RIF1 is a highly conserved
282 protein (Sreesankar et al., 2012) involved in telomeres protection, DNA replication, DNA double-strand
283 break repair, transcription and heterochromatin formation (Mattarocci et al., 2016). The links between
284 the seemingly disparate functions of RIF1 may stem for the function of RIF1 in the stabilization of
285 chromatin topology (Arnould et al., 2021; Klein et al., 2021). Here we provide evidence that the
286 organization of chromatin architecture by RIF1 ensures chromosome stability during DNA replication
287 stress. This model is based on the following findings: (1) RIF1 locates near replication sites in basal
288 conditions (2) DNA replication stress in RIF1-depleted cells modifies S phase patterns and increases the
289 level of the DNA damage marker γH2A.X (3) Suppression of RIF1 strongly affects the organization of
290 DNA replication in response to replicative stress. (4) RIF1 may exert this function in coordination with
291 the cohesin complex. Our model is consistent with the finding that RIF1 bridges proximal DNA
292 molecules (Mattarocci et al., 2017) and creates a protective structure around DBSs (Ochs et al., 2019).
293 Thus, we propose that the chromatin organizing function of RIF1 ensures DNA replication under
294 stressful conditions (Figure 6). By analogy with its function at yeast telomeres, we would like to
295 propose that RIF1 is protecting replication domains (Figure 6).

296 The association of RIF1 with the replication forks has been previously observed by other groups
297 (Alabert et al., 2014; Her et al., 2018; Munden et al., 2018). We confirmed that suppression of RIF1 has
298 no measurable effect on replication forks progression under standard conditions or in response to
299 short treatment with replicative stress (Cornacchia et al., 2012; Ray Chaudhuri et al., 2016; Xu et al.,
300 2010) despite the fact that RIF1 loss induces Chk1 phosphorylation on Ser345 (Chapman et al., 2013;
301 Foti et al., 2016). Interestingly, we found that two hours after release from a thymidine block,
302 replication tracts are longer in the absence of RIF1 and phosphorylation levels of Chk1 on Ser345 and
303 H2A.X on Ser139 are increased. One possibility is that in the absence of RIF1, the disorganization of
304 chromatin domains during DNA replication results in the accumulation of single-stranded DNA. The
305 accumulation of DNA lesions likely underpins the increased sensitivity of RIF1 defective cells to
306 inhibitors of DNA replication (Buonomo et al., 2009; Feng et al., 2013; Xu et al., 2010; Xu et al., 2017).

307 RIF1 is recruited by 53BP1 at DSBs to prevent homologous recombination and favor NHEJ (Chapman
308 et al., 2013; Di Virgilio et al., 2013; Escribano-Diaz et al., 2013; Zimmermann et al., 2013). Based on
309 this, it has been proposed that RIF1 could be recruited by 53BP1 to protect stalled forks independently
310 of BRCA1 (Xu et al., 2017). These data are raising the possibility that 53BP1 contributes to the
311 recruitment of RIF1 at replication forks in basic conditions and in response to replicative stress.
312 However, RIF1 recruitment is not impacted by 53BP1 depletion (Her et al., 2018) and RIF1, but not

313 53BP1, protects nascent DNA from degradation (Ray Chaudhuri et al., 2016) suggesting that the
314 presence of RIF1 at replication forks is independent of 53BP1, consistent with it capacity to form higher
315 order structures in budding yeast (Mattarocci et al., 2017).

316 Our model is consistent with the observation that RIF1 protects stalled replication forks from resection
317 by nucleases, perhaps via the creation of a compartment that prevent their recruitment (Garzón et al.,
318 2019; Mukherjee et al., 2019; Ray Chaudhuri et al., 2016). A role for RIF1 in safeguarding the stability
319 of replicated domains may also explain how RIF1 controls the activation of dormant origins in response
320 to replicative stress (Hiraga et al., 2017) and prevents the formation of anaphase bridges (Hengeveld
321 et al., 2015 ; Zaaijer et al., 2016). RIF1 depletion has a strong impact on replication timing (Cornacchia
322 et al., 2012; Foti et al., 2016; Yamazaki et al., 2012). The action of RIF1 on the replication timing
323 program may result from the regulation of DDK kinase activation through RIF1 interaction with the PP1
324 phosphatase (Dave et al., 2014; Hiraga et al., 2014; Mattarocci et al., 2014) or through its ability to
325 bind G-quadruplexes and to organize chromatin topology (Kanoh et al., 2015). Since the loss of RIF1
326 induces drastic changes in nuclear organization revealed by chromosome conformation capture
327 methods (Foti et al., 2016), we favor the hypothesis that the impact of RIF1 on replication timing is a
328 consequence of impaired nuclear organization rather than of a defect in the control of DDK kinases.
329 The later hypothesis is supported by recent evidence based on Hi-C chromosome conformation
330 capture experiments showing that RIF1 is necessary to enforce chromosome interaction hubs that
331 determine the replication-timing program (Klein et al., 2021). This model could explain why
332 suppression of RIF1 perturbs transcription and heterochromatin formation (Dan et al., 2014; Hiraga et
333 al., 2017; Klein et al., 2021). Since the recruitment of cohesins at stalled forks is dependent on RIF1, it
334 is tempting to speculate that RIF1 might ensures the stabilization of replicating chromatin domains in
335 coordination with cohesin. Consistent with this, the depletion of cohesin subunits mimics topological
336 alterations at DSBs caused by the depletion of RIF1 (Ochs et al., 2019). In contrast, induced degradation
337 of SCC1 did not impact the patterns of replication (Oldach and Nieduszynski, 2019). We favor a model
338 where the cohesin complex is recruited by RIF1 directly at stalled forks to maintain the local
339 organization of chromatin, with no impact on the general organization of DNA replication (Ribeyre et
340 al., 2016; Tittel-Elmer et al., 2012).

341 Finally, this study illustrates an as yet unforeseen application of iPOND (or iPOND-related methods
342 based on formaldehyde crosslinking). It is generally assumed that the iPOND method captures proteins
343 associated with individual replisomes distributed along a linear DNA template. Here we show that the
344 iPOND method is not only efficient to isolate replisome components but also to capture structural
345 components of replicating chromatin domains stabilized by formaldehyde crosslinking. Future studies

346 using iPOND and other method should provide new insights into the role of the nuclear organization
347 in DNA replication.

348

Acknowledgements

We thank all the lab members for comments and suggestions on the project and on the manuscript. We are grateful to Antoine Aze for critical reading of the manuscript. We thank Marie-Pierre Blanchard and the MRI microscopy platform for their support. We acknowledge the support of the Site de Recherche Intégrée sur le Cancer Montpellier Cancer grant INCa_INSERM_DGOS_12553. This work was supported by a Jeunes Chercheuses Jeunes Chercheurs (JCJC) grant (REPLIBLOCK ANR-17-CE12-0034-01) from the Agence National de la Recherche (ANR) to Cyril Ribeyre and by grants from la Fondation ARC pour la Recherche sur le Cancer (PGA1 RF20180206787) and Merck Sharp and Dohme Avenir (GnoSTic) to Angelos Constantinou. Rana Lebdy is funded by fellowships from Azm & Saade Association and Fondation ARC pour la recherche sur le cancer.

Author Contributions

Cyril Ribeyre: conceptualization, data curation, supervision, formal analysis, funding acquisition, investigation, visualization, methodology, project administration and writing original draft, review and editing.

Rana Lebdy: conceptualization, data curation, formal analysis, investigation, visualization, methodology and draft review and editing

Julie Patouillard: formal analysis, investigation, visualization and methodology.

Marion Larroque: data curation, formal analysis, investigation and methodology.

Christian Larroque: data curation, formal analysis and methodology.

Raghida Abou-Merhi: supervision, project administration.

Angelos Constantinou: conceptualization, data curation, supervision, funding acquisition, visualization, methodology, project administration and writing original draft, review and editing.

Conflict of Interest Statement

The authors declare that they have no conflict of interest.

374 **Methods**

375

376 **Cell lines**

377 HeLa S3 (obtained from ATCC) cells were cultured in Dulbecco's modified Eagle's media (DMEM).
378 Culture media was supplemented with 10% fetal bovine serum (Biowest) and penicillin/streptomycin
379 (Sigma-Aldrich). Cells were incubated in a 5% CO_2 at 37°C. For thymidine block experiments cells were
380 treated18 hours with 2 mM thymidine, washed then release into normal media.

381

382 **Gene silencing**

383 For RIF1 depletion siRNA oligonucleotides were purchased from Dharmacon (M-027983-01-0005) and
384 transfected using INTERFERin (Polypus transfection). Anti-RIF1 shRNAs (1) and (2) and anti-luciferase
385 shRNA were cloned in pSUPER-EBV and transfected using Lifofectamine 2000 (Thermo-Fisher). Stable
386 cell lines were selected using puromycin.

387

388 **Western-blot**

389 The proteins were resolved by SDS-PAGE using home-made or precast gels (Bio-Rad) and transferred
390 to a nitrocellulose membrane (GE Healthcare or Bio-Rad). Antibodies against the following proteins
391 were used: Ser345 Phospho-Chk1 (Cell Signaling Technology 2348), Chk1 (Santa Cruz sc-8408), PCNA
392 (Sigma-Aldrich P8825), Ser4/8 Phospho-RPA32 (A300-245A), RPA32 (Calbiochem NA18), TopBP1
393 (Bethyl A300-111A), histone H3 (Abcam ab62642) BRCA1 (Santacruz sc-642), RIF1 (Bethyl A300-568A-
394 M) and MCM7 (Abcam ab2360).

395

396 **Co-Immunoprecipitation**

397 Cells were incubated for 30 min in ice in high salt buffer (50 mM Tris Ph 7.5, 300 mM NaCl, 1% Triton,
398 1 mM DTT). After 10 min centrifugation at 14000g, supernatant was incubated with anti PCNA antibody
399 (Sigma-Aldrich, P8825) or IgG Rabbit (Calbiochem NI01) overnight at 4°C. Magnetic beads coupled with
400 protein G (Life 10004D) were added for 1 hour and washed 5 times with washing buffer (10 mM Hepes,
401 100 mM KOAc, 0.1 mM MgOAc). Beads were boiled in Laemmli buffer and supernatants were analyzed
402 by Western-blot.

403

404 **Isolation of proteins on Nascent DNA (iPOND)**

405 iPOND was performed largely as described in (Lossaint et al., 2013; Ribeyre et al., 2016). Briefly, HeLa
406 S3 cells were pulse labeled with 10 μM EdU for 5-15 min and a 120 min chase was performed with 10
407 μM thymidine. Cells were fixed with 1% formaldehyde for 5 min followed or not by quenching of
408 formaldehyde by 5 min incubation with 0.125 M glycine. Fixed samples were collected by

409 centrifugation at 2000 rpm for 3 min, washed three times with PBS and stored at -80°C. Cells were
410 permeabilized with 0.5% triton and click chemistry was used to conjugate biotin-TEG-azide
411 (Eurogentec) to EdU-labelled DNA. Cells were re-suspended in lysis buffer and sonication was
412 performed using a Qsonica sonicator. Biotin conjugated DNA-protein complexes were captured using
413 streptavidin beads (Ademtech). Captured complexes were washed with lysis buffer and high salt.
414 Proteins associated with nascent DNA were eluted under reducing conditions by boiling into SDS
415 sample buffer for 30 min at 95 °C.
416
417 **DNA fibers labelling**
418 DNA fibers labelling was performed as previously described (Lossaint et al., 2013; Ribeyre et al., 2016).
419 Cells were labeled with 25μM IdU, washed with warm media and exposed to 50 μM CldU. Cells were
420 lysed and DNA fibers were stretched onto glass slides. The DNA fibers were denatured with 2.5 M HCl
421 for 1 hour, washed with PBS and blocked with 2% BSA in PBS-Tween for 60 minutes. IdU replication
422 tracts were revealed with a mouse anti-BrdU/IdU antibody from BD Biosciences (347580) and CldU
423 tracts with a rat anti-BrdU/CldU antibody from Eurobio (ABC117-7513). The following secondary
424 antibodies were used: alexa fluor 488 anti-mouse antibody (Life A21241) and Cy3 anti-rat antibody
425 (Jackson Immunoresearch 712-166-153). Replication tracts lengths were analyzed using ImageJ
426 software. For statistical analysis we used a non-parametrical Mann-Whitney with Prism software.
427
428 **Immunofluorescence**
429 Cells were plated on glass coverslips and fixed with 4% paraformaldehyde in PBS for 20 min at room
430 temperature. When indicated cells were incubated with EdU (5-ethynyl-2'-deoxyuridine) for the
431 indicated times. PFA-fixed cells were permeabilized with 0.2% Triton X-100 in PBS for 5 min. Primary
432 (Ser139 Phospho-H2A.X ; Millipore 05-636 and RIF1 ; Bethyl A300-568A-M) and secondary antibodies
433 (anti-mouse Alexa 488 and anti-rabbit alexa 546) were prepared in PBS with 0.1% Tween and
434 incubations were carried out in a humidified chamber at room temperature (60 min and 30 min,
435 respectively). EdU was coupled with Alexa fluor 555 using Click chemistry. DNA was stained with
436 Hoechst. The cells were mounted on glass slides with Prolong (Life). Cells were analyzed by
437 fluorescence microscopy and quantification of various signals was performed using CellProfiler
438 software (Carpenter et al., 2006).
439
440 **Proximity Ligation Assay**
441 Cells were plated on glass coverslips and fixed with 4% paraformaldehyde in PBS for 20 min at room
442 temperature. When indicated cells were incubated with EdU (5-ethynyl-2'-deoxyuridine). PFA-fixed
443 cells were permeabilized with 0.5% Triton X-100 in PBS for 20 min. EdU was coupled with Alexa fluor

555 or biotin-TEG-azide using Click chemistry. Primary antibodies against SMC1 (Bethyl A300-055A), SMC3 (Bethyl A300-060A), PCNA (Sigma-Aldrich P8825), Biotin (Bethyl A150-109A or Jackson Immunoresearch 200-002-211) were incubated overnight. Probes from Duolink In Situ PLA Probe Anti-Rabbit PLUS (DUO92002, Sigma-Aldrich) and Duolink In Situ PLA Probe Anti-Mouse MINUS (DUO92004, Sigma-Aldrich) we incubated with coverslip 60 min at 37°C. For ligation (30 min at 37°C) and amplification (100 min at 37°C), Duolink In Situ Detection Reagents Green (DUO92014, Sigma-Aldrich) was used. The cells were mounted on glass slides with Duolink In Situ Mounting Medium with DAPI (DUO82040, Sigma-Aldrich). Cells were analyzed by fluorescence microscopy and quantification of PLA signal was performed using CellProfiler software (Carpenter et al., 2006).

Flow cytometry

Cells were labelled with EdU for 15 min then fixed in 80% ethanol. After permeabilization, EdU was coupled with Alexa fluor 488 using Click chemistry. DNA was stained using propidium iodide and analysis was performed on Miltenyi MACS quant device.

Mass Spectrometry Analysis

Mass spectrometry was performed as indicated in (Kumbhar et al., 2018). Analysis of raw files was performed using MaxQuant (Cox and Mann, 2008) version 1.5.6.5 using default settings with label-free quantification option enabled. Raw file spectra were searched against the human UniProt reference database. Protein, peptide, and site false discovery rate (FDR) were adjusted to < 0.01.

465 **References**

466 Alabert, C., Bukowski-Wills, J.C., Lee, S.B., Kustatscher, G., Nakamura, K., de Lima Alves, F., Menard, P.,
467 Mejlvang, J., Rappsilber, J., and Groth, A. (2014). Nascent chromatin capture proteomics determines
468 chromatin dynamics during DNA replication and identifies unknown fork components. Nature cell
469 biology *16*, 281-293.
470 Aranda, S., Rutishauser, D., and Ernfors, P. (2014). Identification of a large protein network involved in
471 epigenetic transmission in replicating DNA of embryonic stem cells. Nucleic acids research *42*, 6972-
472 6986.
473 Arnould, C., Rocher, V., Finoux, A.L., Clouaire, T., Li, K., Zhou, F., Caron, P., Mangeot, P.E., Ricci, E.P.,
474 Mourad, R.*, et al.* (2021). Loop extrusion as a mechanism for formation of DNA damage repair foci.
475 Nature *590*, 660-665.
476 Blow, J.J., Ge, X.Q., and Jackson, D.A. (2011). How dormant origins promote complete genome
477 replication. Trends Biochem Sci *36*, 405-414.
478 Buonomo, S.B., Wu, Y., Ferguson, D., and de Lange, T. (2009). Mammalian Rif1 contributes to
479 replication stress survival and homology-directed repair. J Cell Biol *187*, 385-398.
480 Carpenter, A.E., Jones, T.R., Lamprecht, M.R., Clarke, C., Kang, I.H., Friman, O., Guertin, D.A., Chang,
481 J.H., Lindquist, R.A., Moffat, J.*, et al.* (2006). CellProfiler: image analysis software for identifying and
482 quantifying cell phenotypes. Genome Biol *7*, R100.
483 Chagin, V.O., Casas-Delucchi, C.S., Reinhart, M., Schermelleh, L., Markaki, Y., Maiser, A., Bolius, J.J.,
484 Bensimon, A., Fillies, M., Domaing, P.*, et al.* (2016). 4D Visualization of replication foci in mammalian
485 cells corresponding to individual replicons. Nat Commun *7*, 11231.
486 Chapman, J.R., Barral, P., Vannier, J.B., Borel, V., Steger, M., Tomas-Loba, A., Sartori, A.A., Adams, I.R.,
487 Batista, F.D., and Boulton, S.J. (2013). RIF1 is essential for 53BP1-dependent nonhomologous end
488 joining and suppression of DNA double-strand break resection. Molecular cell *49*, 858-871.
489 Cobb, A.M., Murray, T.V., Warren, D.T., Liu, Y., and Shanahan, C.M. (2016). Disruption of PCNA-lamins
490 A/C interactions by prelamin A induces DNA replication fork stalling. Nucleus *7*, 498-511.
491 Cornacchia, D., Dileep, V., Quivy, J.P., Foti, R., Tili, F., Santarella-Mellwig, R., Antony, C., Almouzni, G.,
492 Gilbert, D.M., and Buonomo, S.B. (2012). Mouse Rif1 is a key regulator of the replication-timing
493 programme in mammalian cells. The EMBO journal *31*, 3678-3690.
494 Courbet, S., Gay, S., Arnoult, N., Wronka, G., Anglana, M., Brison, O., and Debatisse, M. (2008).
495 Replication fork movement sets chromatin loop size and origin choice in mammalian cells. Nature *455*,
496 557-560.
497 Cox, J., and Mann, M. (2008). MaxQuant enables high peptide identification rates, individualized p.p.b.-
498 range mass accuracies and proteome-wide protein quantification. Nat Biotechnol *26*, 1367-1372.

499 Dan, J., Liu, Y., Liu, N., Chiourea, M., Okuka, M., Wu, T., Ye, X., Mou, C., Wang, L., Wang, L.*, et al.* (2014).
500 Rif1 maintains telomere length homeostasis of ESCs by mediating heterochromatin silencing.
501 Developmental cell *29*, 7-19.
502 Dave, A., Cooley, C., Garg, M., and Bianchi, A. (2014). Protein phosphatase 1 recruitment by Rif1
503 regulates DNA replication origin firing by counteracting DDK activity. Cell reports *7*, 53-61.
504 Davidson, I.F., Bauer, B., Goetz, D., Tang, W., Wutz, G., and Peters, J.-M. (2019). DNA loop extrusion by
505 human cohesin. Science *366*, 1338-1345.
506 Di Virgilio, M., Callen, E., Yamane, A., Zhang, W., Jankovic, M., Gitlin, A.D., Feldhahn, N., Resch, W.,
507 Oliveira, T.Y., Chait, B.T.*, et al.* (2013). Rif1 prevents resection of DNA breaks and promotes
508 immunoglobulin class switching. Science *339*, 711-715.
509 Dimitrova, D.S., and Berezney, R. (2002). The spatio-temporal organization of DNA replication sites is
510 identical in primary, immortalized and transformed mammalian cells. J Cell Sci *115*, 4037-4051.
511 Dungrawala, H., Rose, K.L., Bhat, K.P., Mohni, K.N., Glick, G.G., Couch, F.B., and Cortez, D. (2015). The
512 Replication Checkpoint Prevents Two Types of Fork Collapse without Regulating Replisome Stability.
513 Molecular cell *59*, 998-1010.
514 Escribano-Diaz, C., Orthwein, A., Fradet-Turcotte, A., Xing, M., Young, J.T., Tkac, J., Cook, M.A.,
515 Rosebrock, A.P., Munro, M., Canny, M.D.*, et al.* (2013). A cell cycle-dependent regulatory circuit
516 composed of 53BP1-RIF1 and BRCA1-CtIP controls DNA repair pathway choice. Molecular cell *49*, 872-
517 883.
518 Feng, L., Fong, K.W., Wang, J., Wang, W., and Chen, J. (2013). RIF1 counteracts BRCA1-mediated end
519 resection during DNA repair. The Journal of biological chemistry *288*, 11135-11143.
520 Foti, R., Gnan, S., Cornacchia, D., Dileep, V., Bulut-Karslioglu, A., Diehl, S., Buness, A., Klein, F.A., Huber,
521 W., Johnstone, E.*, et al.* (2016). Nuclear Architecture Organized by Rif1 Underpins the Replication-
522 Timing Program. Molecular cell *61*, 260-273.
523 Garzón, J., Ursich, S., Lopes, M., Hiraga, S.-i., and Donaldson, A.D. (2019). Human RIF1-Protein
524 Phosphatase 1 Prevents Degradation and Breakage of Nascent DNA on Replication Stalling. Cell reports
525 *27*, 2558-2566.e2554.
526 Guillou, E., Ibarra, A., Coulon, V., Casado-Vela, J., Rico, D., Casal, I., Schwob, E., Losada, A., and Mendez,
527 J. (2010). Cohesin organizes chromatin loops at DNA replication factories. Genes & development *24*,
528 2812-2822.
529 Hardy, C.F., Sussel, L., and Shore, D. (1992). A RAP1-interacting protein involved in transcriptional
530 silencing and telomere length regulation. Genes & development *6*, 801-814.
531 Hayano, M., Kanoh, Y., Matsumoto, S., Renard-Guillet, C., Shirahige, K., and Masai, H. (2012). Rif1 is a
532 global regulator of timing of replication origin firing in fission yeast. Genes & development *26*, 137-
533 150.

534 Hengeveld, R.C., de Boer, H.R., Schoonen, P.M., de Vries, E.G., Lens, S.M., and van Vugt, M.A. (2015).
535 Rif1 Is Required for Resolution of Ultrafine DNA Bridges in Anaphase to Ensure Genomic Stability.
536 Developmental cell *34*, 466-474.
537 Her, J., Ray, C., Altshuler, J., Zheng, H., and Bunting, S.F. (2018). 53BP1 Mediates ATR-Chk1 Signaling
538 and Protects Replication Forks under Conditions of Replication Stress. Mol Cell Biol *38*.
539 Hiraga, S., Alvino, G.M., Chang, F., Lian, H.Y., Sridhar, A., Kubota, T., Brewer, B.J., Weinreich, M.,
540 Raghuraman, M.K., and Donaldson, A.D. (2014). Rif1 controls DNA replication by directing Protein
541 Phosphatase 1 to reverse Cdc7-mediated phosphorylation of the MCM complex. Genes &
542 development *28*, 372-383.
543 Hiraga, S.I., Ly, T., Garzon, J., Horejsi, Z., Ohkubo, Y.N., Endo, A., Obuse, C., Boulton, S.J., Lamond, A.I.,
544 and Donaldson, A.D. (2017). Human RIF1 and protein phosphatase 1 stimulate DNA replication origin
545 licensing but suppress origin activation. EMBO reports *18*, 403-419.
546 Kanoh, Y., Matsumoto, S., Fukatsu, R., Kakusho, N., Kono, N., Renard-Guillet, C., Masuda, K., Iida, K.,
547 Nagasawa, K., Shirahige, K.*, et al.* (2015). Rif1 binds to G quadruplexes and suppresses replication over
548 long distances. Nat Struct Mol Biol *22*, 889-897.
549 Kim, Y., Shi, Z., Zhang, H., Finkelstein, I.J., and Yu, H. (2019). Human cohesin compacts DNA by loop
550 extrusion. Science *366*, 1345-1349.
551 Klein, K.N., Zhao, P.A., Lyu, X., Sasaki, T., Bartlett, D.A., Singh, A.M., Tasan, I., Zhang, M., Watts, L.P.,
552 Hiraga, S.I.*, et al.* (2021). Replication timing maintains the global epigenetic state in human cells.
553 Science *372*, 371-378.
554 Kumbhar, R., Vidal-Eychenié, S., Kontopoulos, D.-G., Larroque, M., Larroque, C., Basbous, J., Kossida,
555 S., Ribeyre, C., and Constantinou, A. (2018). Recruitment of ubiquitin-activating enzyme UBA1 to DNA
556 by poly(ADP-ribose) promotes ATR signalling. Life Science Alliance *1*.
557 Kurose, A., Tanaka, T., Huang, X., Traganos, F., and Darzynkiewicz, Z. (2006). Synchronization in the cell
558 cycle by inhibitors of DNA replication induces histone H2AX phosphorylation: an indication of DNA
559 damage. Cell Prolif *39*, 231-240.
560 Lambert, S., and Carr, A.M. (2013). Impediments to replication fork movement: stabilisation,
561 reactivation and genome instability. Chromosoma *122*, 33-45.
562 Lopez-Contreras, A.J., Ruppen, I., Nieto-Soler, M., Murga, M., Rodriguez-Acebes, S., Remeseiro, S.,
563 Rodrigo-Perez, S., Rojas, A.M., Mendez, J., Munoz, J.*, et al.* (2013). A proteomic characterization of
564 factors enriched at nascent DNA molecules. Cell reports *3*, 1105-1116.
565 Lossaint, G., Larroque, M., Ribeyre, C., Bec, N., Larroque, C., Decaillet, C., Gari, K., and Constantinou,
566 A. (2013). FANCD2 binds MCM proteins and controls replisome function upon activation of s phase
567 checkpoint signaling. Molecular cell *51*, 678-690.

568 Marchal, C., Sima, J., and Gilbert, D.M. (2019). Control of DNA replication timing in the 3D genome.
569 Nat Rev Mol Cell Biol *20*, 721-737.
570 Mattarocci, S., Hafner, L., Lezaja, A., Shyian, M., and Shore, D. (2016). Rif1: A Conserved Regulator of
571 DNA Replication and Repair Hijacked by Telomeres in Yeasts. Frontiers in genetics *7*, 45.
572 Mattarocci, S., Reinert, J.K., Bunker, R.D., Fontana, G.A., Shi, T., Klein, D., Cavadini, S., Faty, M., Shyian,
573 M., Hafner, L.*, et al.* (2017). Rif1 maintains telomeres and mediates DNA repair by encasing DNA ends.
574 Nat Struct Mol Biol *24*, 588-595.
575 Mattarocci, S., Shyian, M., Lemmens, L., Damay, P., Altintas, D.M., Shi, T., Bartholomew, C.R., Thoma,
576 N.H., Hardy, C.F., and Shore, D. (2014). Rif1 controls DNA replication timing in yeast through the PP1
577 phosphatase Glc7. Cell reports *7*, 62-69.
578 Mechali, M. (2010). Eukaryotic DNA replication origins: many choices for appropriate answers. Nat Rev
579 Mol Cell Biol *11*, 728-738.
580 Moriyama, K., Yoshizawa-Sugata, N., and Masai, H. (2018). Oligomer formation and G-quadruplex
581 binding by purified murine Rif1 protein, a key organizer of higher-order chromatin architecture. The
582 Journal of biological chemistry *293*, 3607-3624.
583 Mukherjee, C., Tripathi, V., Manolika, E.M., Heijink, A.M., Ricci, G., Merzouk, S., de Boer, H.R.,
584 Demmers, J., van Vugt, M.A.T.M., and Ray Chaudhuri, A. (2019). RIF1 promotes replication fork
585 protection and efficient restart to maintain genome stability. Nature Communications *10*, 3287.
586 Munden, A., Rong, Z., Sun, A., Gangula, R., Mallal, S., and Nordman, J.T. (2018). Rif1 inhibits replication
587 fork progression and controls DNA copy number in Drosophila. Elife *7*.
588 Ochs, F., Karemore, G., Miron, E., Brown, J., Sedlackova, H., Rask, M.-B., Lampe, M., Buckle, V.,
589 Schermelleh, L., Lukas, J.*, et al.* (2019). Stabilization of chromatin topology safeguards genome
590 integrity. Nature *574*, 571-574.
591 Oldach, P., and Nieduszynski, C.A. (2019). Cohesin-Mediated Genome Architecture Does Not Define
592 DNA Replication Timing Domains. Genes (Basel) *10*.
593 Petruk, S., Cai, J., Sussman, R., Sun, G., Kovermann, S.K., Mariani, S.A., Calabretta, B., McMahon, S.B.,
594 Brock, H.W., Iacovitti, L.*, et al.* (2017). Delayed Accumulation of H3K27me3 on Nascent DNA Is Essential
595 for Recruitment of Transcription Factors at Early Stages of Stem Cell Differentiation. Molecular cell *66*,
596 247-257 e245.
597 Petruk, S., Sedkov, Y., Johnston, D.M., Hodgson, J.W., Black, K.L., Kovermann, S.K., Beck, S., Canaani,
598 E., Brock, H.W., and Mazo, A. (2012). TrxG and PcG proteins but not methylated histones remain
599 associated with DNA through replication. Cell *150*, 922-933.
600 Ray Chaudhuri, A., Callen, E., Ding, X., Gogola, E., Duarte, A.A., Lee, J.E., Wong, N., Lafarga, V., Calvo,
601 J.A., Panzarino, N.J.*, et al.* (2016). Replication fork stability confers chemoresistance in BRCA-deficient
602 cells. Nature *535*, 382-387.

603 Ribeyre, C., Zellweger, R., Chauvin, M., Bec, N., Larroque, C., Lopes, M., and Constantinou, A. (2016).
604 Nascent DNA Proteomics Reveals a Chromatin Remodeler Required for Topoisomerase I Loading at
605 Replication Forks. Cell reports *15*, 300-309.
606 Roy, S., Luzwick, J.W., and Schlacher, K. (2018). Correction: SIRF: Quantitative in situ analysis of protein
607 interactions at DNA replication forks. J Cell Biol *217*, 1553.
608 Singh, M., Hunt, C.R., Pandita, R.K., Kumar, R., Yang, C.R., Horikoshi, N., Bachoo, R., Serag, S., Story,
609 M.D., Shay, J.W.*, et al.* (2013). Lamin A/C depletion enhances DNA damage-induced stalled replication
610 fork arrest. Mol Cell Biol *33*, 1210-1222.
611 Sirbu, B.M., Couch, F.B., Feigerle, J.T., Bhaskara, S., Hiebert, S.W., and Cortez, D. (2011). Analysis of
612 protein dynamics at active, stalled, and collapsed replication forks. Genes & development *25*, 1320-
613 1327.
614 Sirbu, B.M., McDonald, W.H., Dungrawala, H., Badu-Nkansah, A., Kavanaugh, G.M., Chen, Y., Tabb, D.L.,
615 and Cortez, D. (2013). Identification of proteins at active, stalled, and collapsed replication forks using
616 isolation of proteins on nascent DNA (iPOND) coupled with mass spectrometry. The Journal of
617 biological chemistry *288*, 31458-31467.
618 Sreesankar, E., Senthilkumar, R., Bharathi, V., Mishra, R.K., and Mishra, K. (2012). Functional
619 diversification of yeast telomere associated protein, Rif1, in higher eukaryotes. BMC genomics *13*, 255.
620 Tittel-Elmer, M., Lengronne, A., Davidson, M.B., Bacal, J., Francois, P., Hohl, M., Petrini, J.H., Pasero, P.,
621 and Cobb, J.A. (2012). Cohesin association to replication sites depends on rad50 and promotes fork
622 restart. Molecular cell *48*, 98-108.
623 Tyanova, S., Temu, T., Sinitcyn, P., Carlson, A., Hein, M.Y., Geiger, T., Mann, M., and Cox, J. (2016). The
624 Perseus computational platform for comprehensive analysis of (prote)omics data. Nat Methods *13*,
625 731-740.
626 Wheaton, K., Campuzano, D., Ma, W., Sheinis, M., Ho, B., Brown, G.W., and Benchimol, S. (2017).
627 Progerin-Induced Replication Stress Facilitates Premature Senescence in Hutchinson-Gilford Progeria
628 Syndrome. Mol Cell Biol *37*.
629 Xu, D., Muniandy, P., Leo, E., Yin, J., Thangavel, S., Shen, X., Ii, M., Agama, K., Guo, R., Fox, D., 3rd*, et*
630 *al.* (2010). Rif1 provides a new DNA-binding interface for the Bloom syndrome complex to maintain
631 normal replication. The EMBO journal *29*, 3140-3155.
632 Xu, Y., Ning, S., Wei, Z., Xu, R., Xu, X., Xing, M., Guo, R., and Xu, D. (2017). 53BP1 and BRCA1 control
633 pathway choice for stalled replication restart. Elife *6*.
634 Yamazaki, S., Hayano, M., and Masai, H. (2013). Replication timing regulation of eukaryotic replicons:
635 Rif1 as a global regulator of replication timing. Trends Genet *29*, 449-460.
636 Yamazaki, S., Ishii, A., Kanoh, Y., Oda, M., Nishito, Y., and Masai, H. (2012). Rif1 regulates the replication
637 timing domains on the human genome. The EMBO journal *31*, 3667-3677.

638 Zaaijer, S., Shaikh, N., Nageshan, R.K., and Cooper, J.P. (2016). Rif1 Regulates the Fate of DNA
639 Entanglements during Mitosis. Cell reports *16*, 148-160.
640 Zeman, M.K., and Cimprich, K.A. (2014). Causes and consequences of replication stress. Nature cell
641 biology *16*, 2-9.
642 Zimmermann, M., Lottersberger, F., Buonomo, S.B., Sfeir, A., and de Lange, T. (2013). 53BP1 regulates
643 DSB repair using Rif1 to control 5' end resection. Science *339*, 700-704.

644

645

646

647

648

649

650

651

652

653

654

655

656

657

658 **Figures Legends**

659 **Figure 1: RIF1 is associated with nascent DNA and is required to limit DNA lesions in response to**
660 **prolonged aphidicolin treatment. A.** iPOND coupled with mass spectrometry. HeLa S3 were pulse-
661 labeled with EdU or pulse-labelled with EdU then subjected to a 120 min thymidine chase the subjected
662 to iPOND and analyzed by mass-spectrometry. Label free quantification was performed using
663 MaxQuant (Cox and Mann, 2008) and statistical analysis using Perseus (Tyanova et al., 2016). Pulse
664 experiments have been performed 6 times and chase experiments 4 times. Examples of replisome-
665 specific proteins are indicated on the right side of the figure above the line. Full proteins list is available
666 in Supplementary Table 1. **B.** Indicated proteins were isolated by iPOND and detected by Western
667 blotting. HeLa S3 cells were pulse-labelled with EdU for 15 min and chased with thymidine for 120 min.
668 In no click biotin-TEG azide was replaced by DMSO. **C.** Western-blot analysis of indicated proteins after
669 immunoprecipitation with an antibody directed against PCNA or against mouse IgG. **D.** DNA fibers
670 labelling and Western-blot analysis of RIF1 depletion. HeLa S3 cells were labelled for 30 min with IdU
671 and then for 30 min with CldU in the absence or presence of 0.05 μM aphidicolin (APH) in the cell
672 culture medium. Graphic representation of the ratios of CldU versus IdU tract length. For statistical
673 analysis Mann-Whitney test was used; ns, non-significant, ****$p<0.0001$. The horizontal bar
674 represents the median with the value indicated in red. 50 replication tracts were measured for each
675 experimental condition. **E.** Analysis of DNA resection using DNA fibers labelling. HeLa S3 cells were
676 labelled for 30 min with IdU and then for 30 min with CldU. 1 μM aphidicolin (APH) was added in the
677 cell culture medium for 6 hours. Graphic representation of the ratios of CldU versus IdU tract length.
678 For statistical analysis Mann-Whitney test was used; ****$p<0.0001$. The horizontal bar represents the
679 median with the value indicated in red. 50 replication tracts were measured for each experimental
680 condition. **F.** Immunofluorescence analysis of γH2A.X and RIF1 in HeLa S3 cells with siRNA against
681 control or RIF1 in presence or absence of aphidicolin (APH) for 24 hours. Graphic representation of the
682 percentage of γH2A.X positive cells based on 3 independent experiments.

683 **Figure 2: RIF1 depletion alters S-phase organization and yields DNA lesions. A.** Experimental setup to
684 study the impact of synchronization procedure in HeLa S3 cells depleted or not for RIF1. The efficacy
685 of RIF1 depletion using 2 different shRNA is shown. For synchronization, cells were grown 18 hours in
686 presence of 2mM thymidine then released into S-phase for 2 hours. Cells were then subjected to
687 immunofluorescence, western-blot or DNA fibers analysis. **B.** Immunofluorescence analysis of γH2A.X
688 and EdU in asynchronous and synchronous HeLa S3 cells expressing shRNAs against luciferase or RIF1.
689 **C.** Graphic representation of the frequency of replication patterns (Late-S, Mid-S and Early-S) based on
690 at least three independent experiments for each condition. **D.** Quantification of γH2A.X intensity within
691 nucleus stained with Hoechst using CellProfiler based on at least three independent experiments for

692 each condition. **E.** Western-blot analysis of Chk1 phosphorylation on Serine 345 upon RIF1 depletion
693 **E.** DNA fibers assay. HeLa S3 cells were labelled for 30 min with IdU and then for 30 min with CldU.
694 Graphic representation of CldU tracts lengths. For statistical analysis Mann-Whitney test was used; ns,
695 non-significant, ****p<0.0001. The horizontal bar represents the median with the value indicated in
696 red. At least 50 replication tracts were measured for each experimental condition.

697 **Figure 3: RIF1 loss reduces the efficacy of proteins isolation on nascent DNA. A.** Experimental set-up.
698 **B.** iPOND experiment. HeLa S3 cells (with shLUC or two different shRIF1) were labelled with EdU for 15
699 min or for 30 min with 0.1 μM aphidicolin (APH). Indicated proteins were analyzed by western-blotting.
700 In no click samples biotin-TEG azide was replaced by DMSO. **C.** Analysis of EdU incorporation using
701 microscopy in HeLa S3 cells with shRNA against luciferase or RIF1. EdU was incorporated in cells during
702 15 min with or without 0.1 μM aphidicolin (APH). Quantification of EdU intensity within nucleus stained
703 with Hoechst was performed using CellProfiler and is represented on the histogram. Error-bars
704 corresponds to the average values of three independent experiments. **D.** DNA fibers labelling. HeLa S3
705 cells were labelled for 30 min with IdU and then for 30 min with CldU in the absence or presence of
706 0.05 μM aphidicolin (APH) in the cell culture medium. Graphic representation of the ratios of CldU
707 versus IdU tract length. For statistical analysis Mann-Whitney test was used; ****p<0.0001. The
708 horizontal bar represents the median with the value indicated in red. At least 50 replication tracts were
709 measured for each experimental condition. **E.** iPOND-MS experiment. HeLa S3 cells (with shLUC or two
710 different shRIF1) were labelled with EdU for 15 min or for 30 min EdU with 0.1 μM aphidicolin (APH).
711 Quantification of peptides intensity corresponding to the indicated proteins is represented.

712 **Figure 4: iPOND proteins recovery is biased by replication organization. A.** Experimental set-up. HeLa
713 S3 cells were submitted to thymidine block during 18 hours and released into S-phase. Cells were
714 collected at T0 (G1), T2 (Early-S), T4 (Mid-S) and T8 (Late-S) after 15 min EdU pulse for iPOND and flow
715 cytometry. Replication patterns showing the different phases are represented. **B.** The percentage of
716 cells in each phase was analyzed using flow cytometry. The error-bars represent the variations within
717 3 independent experiments. **C.** iPOND experiment performed on unsynchronized and synchronized
718 cells and analyzed by western-blot using antibodies directed against the indicated proteins. In no click
719 samples, biotin-TEG azide was replaced by DMSO. **D.** Quantification of the indicated proteins in iPOND
720 based on at least 3 independent experiments, T0 was used for normalization.

721 **Figure 5: RIF1 is required for full recruitment of cohesin subunits at stalled forks. A.** Scheme
722 explaining the principle of proximity ligation assay (PLA) between EdU and replisome components. **B.**
723 Immunofluorescence analysis of PLA signal between EdU and SMC1 and between EdU and PCNA upon
724 30 min treatment with 0.1 μM APH in HeLa S3 cells expressing shRNAs against luciferase or RIF1. EdU-

725 positive cells were labelled with Alexa-Fluor 555. **C.** The level of PLA signal within the nucleus was
726 quantified using CellProfiler. Graphical representation of the PLA signal, at least 100 cells were
727 quantified in each condition. For statistical analysis Mann-Whitney test was used; ns, non-significant,
728 ****$p<0.0001$; ***$p<0.001$.

729 **Figure 6: Model to explain the role of RIF1 in the organization of replication factories.** RIF1 stabilizes
730 chromatin topology during DNA replication thus preventing DNA resection by nucleases or excessive
731 origins activation. This could direct, thanks to its capacity to interact with DNA, or/and via the
732 recruitment of cohesin ring. In its absence, the replication domains are unprotected leading to DNA
733 resection, DNA lesions and activation of DNA damage response.

734

735 **Supplementary figures legends**

736 **Sup Figure 1: A.** DNA fibers labelling. HeLa S3 cells were labelled for 30 min with IdU and then for 30
737 min with CldU. Graphic representation of the ratios of CldU tract length. The horizontal bar represents
738 the median with the value indicated in red. For statistical analysis Mann-Whitney test was used; ns,
739 non-significant. At least 50 replication tracts were measured for each experimental condition. The
740 second graphic representation is showing the average of four independent experiments. **B.** Western-
741 blot analysis of the indicated proteins upon transfection with siRNA directed against RIF1 or a control
742 target. **C.** This graphic representation is showing the average of the three independent experiments
743 from Figure 1D. **D.** Analysis of replication restart upon APH treatment using DNA fibers labelling. HeLa
744 S3 cells were labelled for 30 min with IdU, then treated 16 hrs with 10μM APH and then for 30 min
745 with CldU. Graphic representation of the percentage of restart based on 3 independent experiments.

746 **Sup Figure 2: A.** Flow cytometry analysis of cells depleted or not for RIF1 in asynchronous or
747 synchronous conditions (18 hours thymidine block followed by 2 hours release). DNA was stained using
748 propidium iodide. **B.** This graphic representation is showing the average of the three independent
749 experiments from Figure 2F.

750 **Sup Figure 3: A.** iPOND experiment. HeLa S3 cells (with shLUC or two different shRIF1) were treated
751 30 min with 0.1 μM aphidicolin (APH) then washed and labelled with EdU for 30 min. Indicated proteins
752 were analyzed by Western-blotting. In no click samples, biotin-TEG azide was replaced by DMSO. **B.**
753 Western-blot analysis of indicated proteins after immunoprecipitation with an antibody directed
754 against PCNA or against mouse IgG. When indicated HeLa S3 cells (shLUc or shRIF1) were treated for
755 30 min with 0.1 μM aphidicolin (APH). **C.** Peptides intensity of proteins not specific from the replisome
756 from the iPOND experiment from Figure 3C. **D.** Summed intensities of peptides corresponding to
757 replisomes components (listed in Supplementary Table 2)from the iPOND experiment from Figure 3C.

758 **Sup Figure 4:** Scheme explaining how replication organization is impacting iPOND efficiency.

759 **Sup Figure 5: A.** Immunofluorescence analysis of PLA signal between EdU and PCNA, in -click control
760 the Biotin-TEG azide was replaced by DMSO. **B.** Graphic representation of the average PLA signal
761 (normalized to 100 in shLUC) from 3 independent experiments corresponding to Figure 5C. **C.**
762 Immunofluorescence analysis of PLA signal between EdU and SMC3 upon 30 min treatment with 0.1
763 μM APH in HeLa S3 cells expressing shRNAs against luciferase or RIF1. EdU-positive cells were labelled
764 with Alexa-Fluor 555. The level of PLA signal within the nucleus was quantified using CellProfiler.
765 Graphical representation of the PLA signal, at least 100 cells were quantified in each condition. For
766 statistical analysis Mann-Whitney test was used; ****$p<0.0001$. Graphic representation of the average

767 PLA signal (normalized to 100 in shLUC) from 3 independent experiments. **A.** Immunofluorescence
768 analysis of SMC1 and SMC3. Graphic representation of the average SMC1 and SMC3 intensity within
769 nucleus (normalized to 100 in shLUC) from 3 independent experiments.

770

771

772

773

774

775

776

777

778

779

780

781

782

783

Figure 1

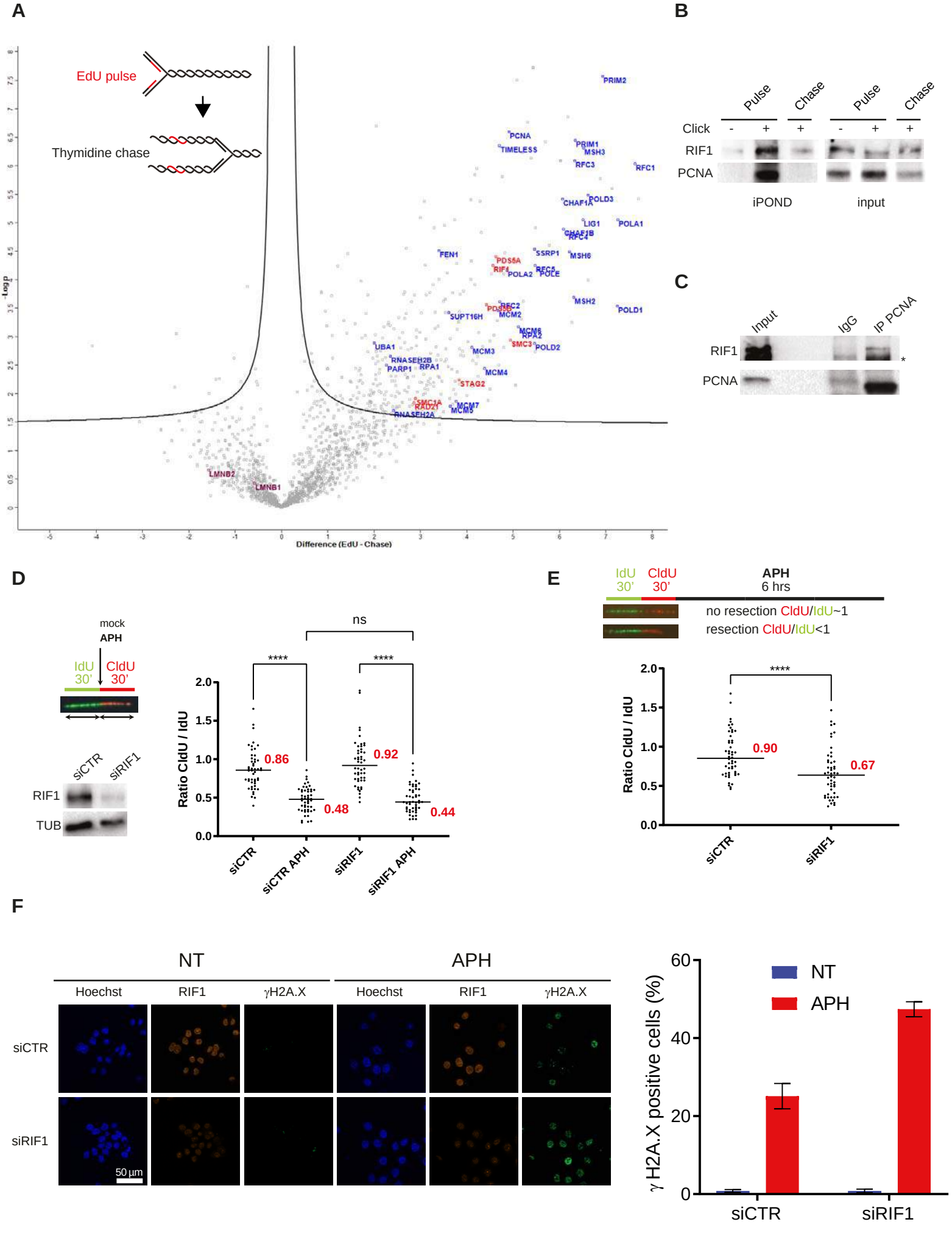
A
EdU pulse
Thymidine chase
-Log P
Difference (EdU - Chase)
PRIM2
PCNA
TIMELESS
PRIM1
MSH3
RFC3
RFC1
CHAF1A
POLD3
LIG1
POLA1
CHAF1B
RFC4
FEN1
SSRP1
MSH6
PDS5A
RIF1
POLA2
RFC5
POLE
MSH2
POLD1
RFC2
MCM2
SUPT16H
MCM6
RPA2
SMC3
POLD2
UBA1
MCM3
RNASEH2B
PARP1
RPA1
MCM4
STAG2
SMC1A
RAD21
MCM7
MCM5
RNASEH2A
LMNB2
LMNB1
B
Pulse
Chase
Pulse
Chase
Click
RIF1
PCNA
iPOND
input
C
Input
IgG
IP PCNA
RIF1
PCNA
D
mock
APH
IdU 30'
CldU 30'
siCTR
siRIF1
RIF1
TUB
ns
****
****
Ratio CldU / IdU
0.86
0.48
0.92
0.44
siCTR
siCTR APH
siRIF1
siRIF1 APH
E
IdU 30'
CldU 30'
APH 6 hrs
no resection CldU/IdU~1
resection CldU/IdU<1
****
Ratio CldU / IdU
0.90
0.67
siCTR
siRIF1
F
NT
APH
Hoechst
RIF1
γH2A.X
Hoechst
RIF1
γH2A.X
siCTR
siRIF1
50 µm
NT
APH
γ H2A.X positive cells (%)
siCTR
siRIF1

Figure 2

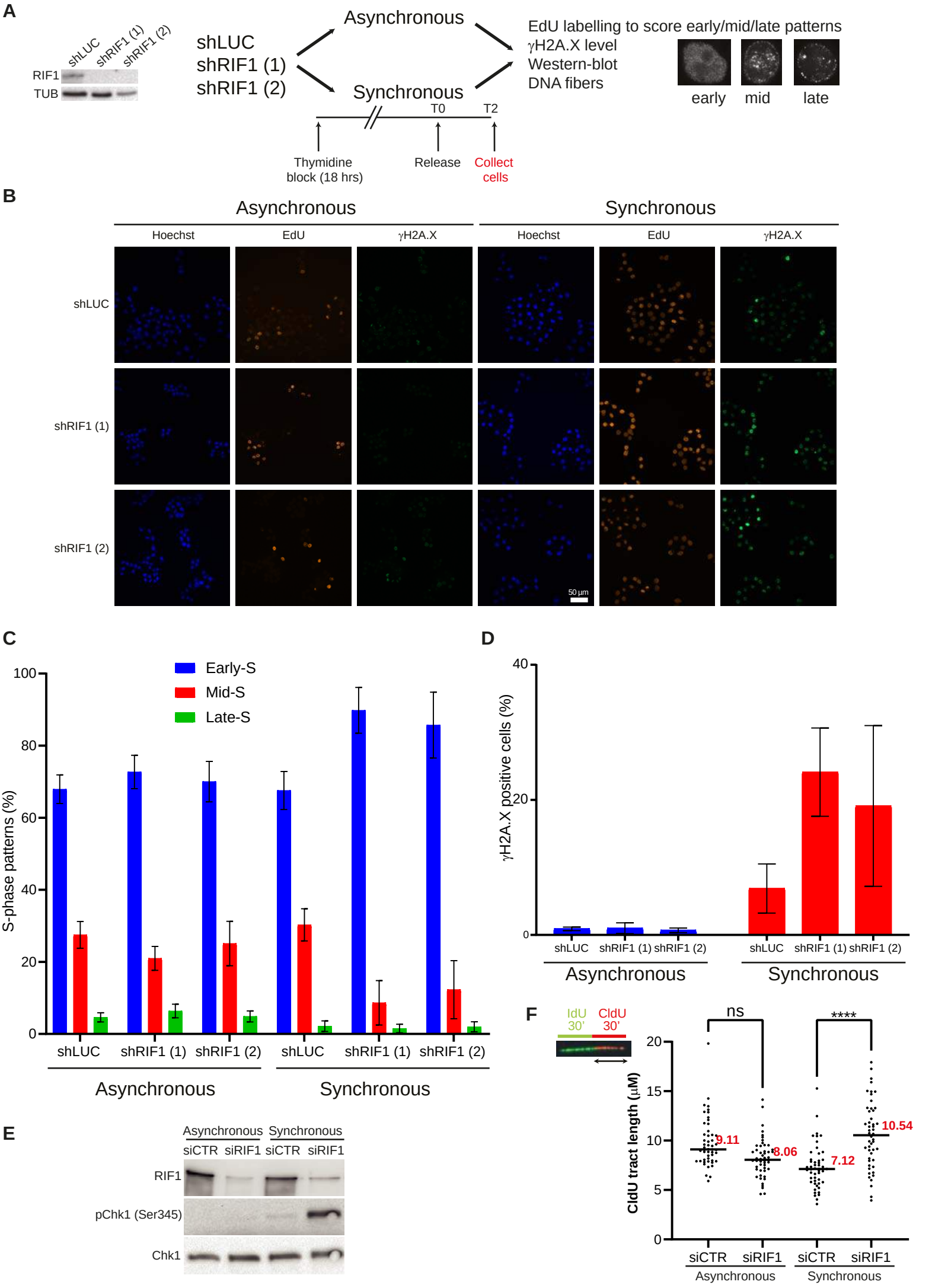
A
shLUC
shRIF1 (1)
shRIF1 (2)
RIF1
TUB
shLUC
shRIF1 (1)
shRIF1 (2)
Asynchronous
Synchronous
T0
T2
Thymidine block (18 hrs)
Release
Collect cells
EdU labelling to score early/mid/late patterns
γH2A.X level
Western-blot
DNA fibers
early
mid
late
B
Asynchronous
Synchronous
Hoechst
EdU
γH2A.X
shLUC
shRIF1 (1)
shRIF1 (2)
50 µm
C
Early-S
Mid-S
Late-S
S-phase patterns (%)
shLUC
shRIF1 (1)
shRIF1 (2)
Asynchronous
Synchronous
D
γH2A.X positive cells (%)
shLUC
shRIF1 (1)
shRIF1 (2)
Asynchronous
Synchronous
E
Asynchronous
Synchronous
siCTR
siRIF1
RIF1
pChk1 (Ser345)
Chk1
F
IdU 30'
CldU 30'
ns
****
CldU tract length (µM)
9.11
8.06
7.12
10.54
siCTR
siRIF1
Asynchronous
Synchronous

Figure 3

A

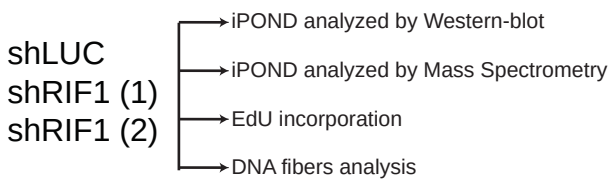

B

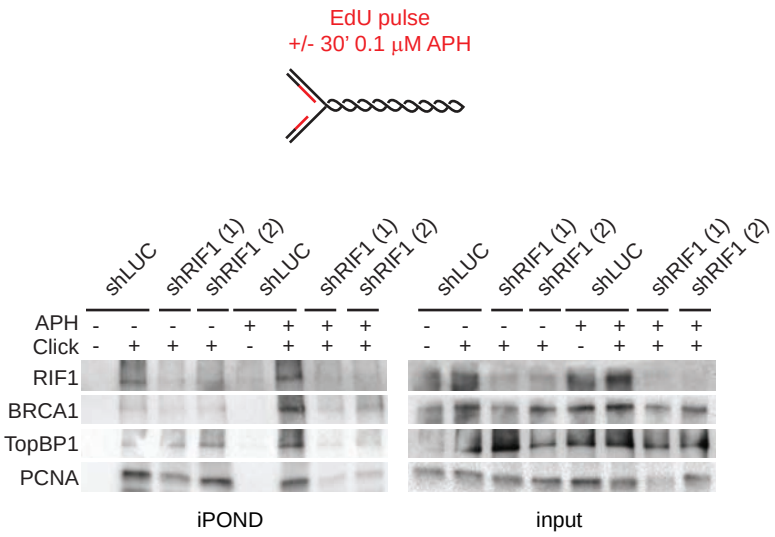

E

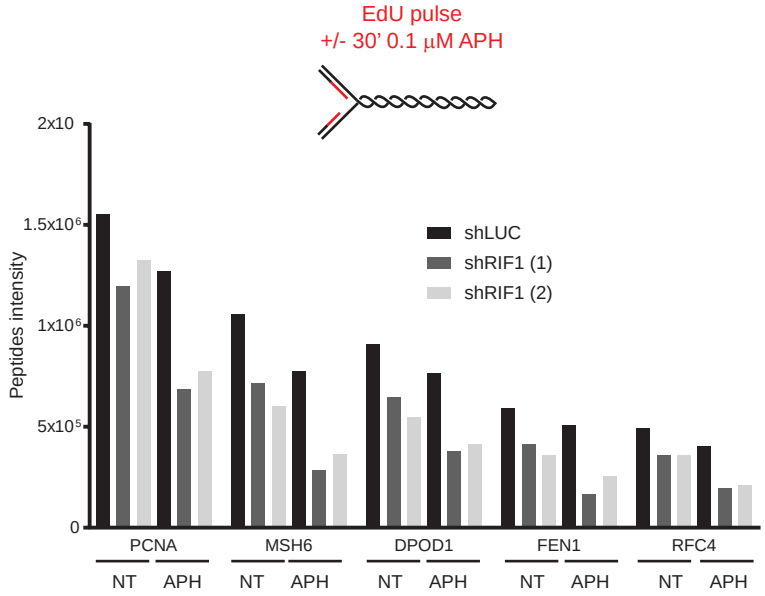

C

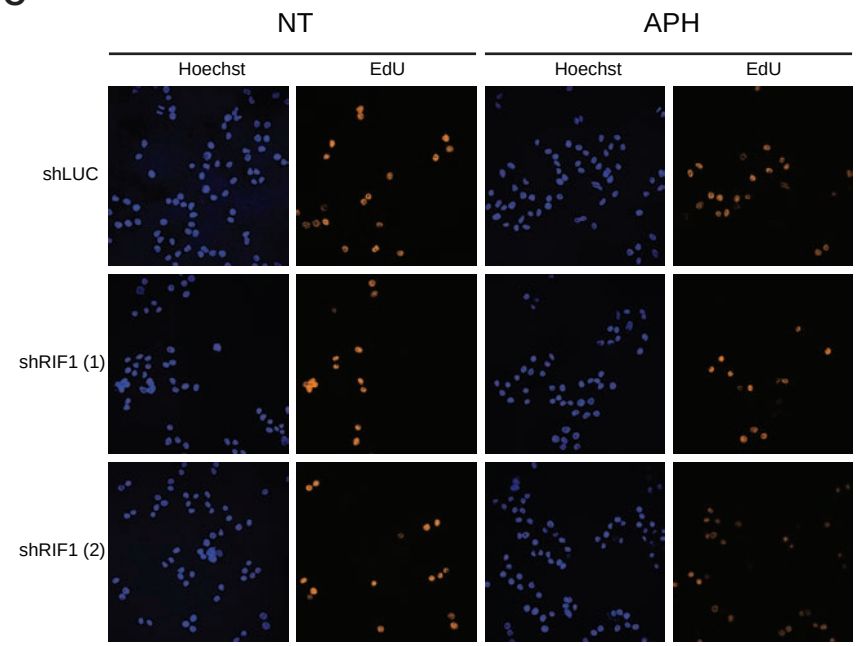

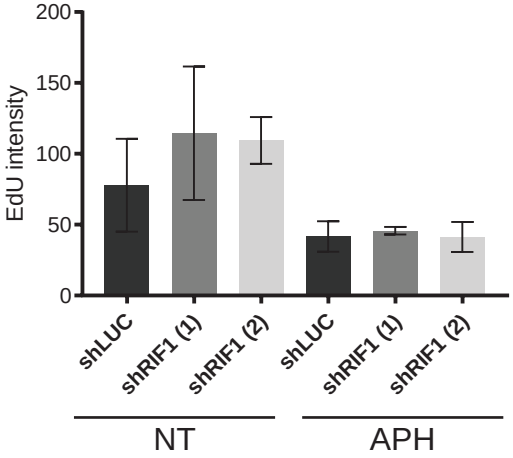

D

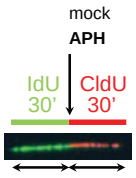

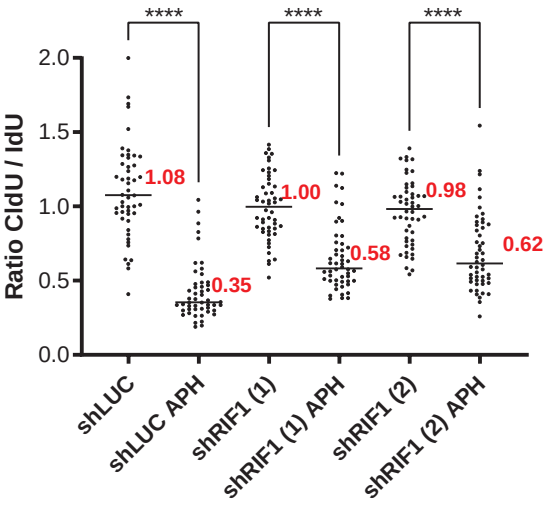

Figure 4

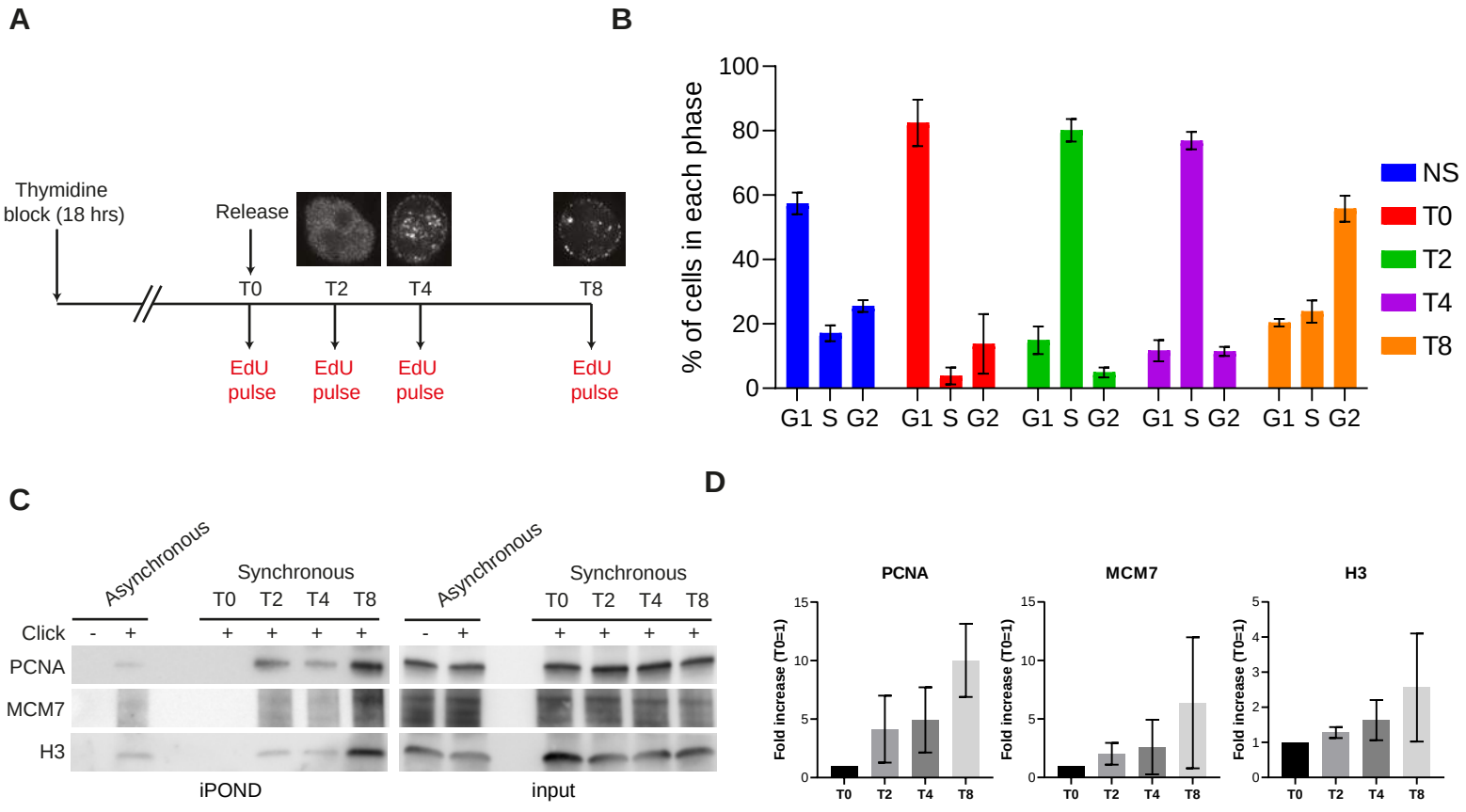
A
Thymidine block (18 hrs)
Release
T0
T2
T4
T8
EdU pulse
EdU pulse
EdU pulse
EdU pulse
B
% of cells in each phase
100
80
60
40
20
0
G1 S G2 G1 S G2 G1 S G2 G1 S G2 G1 S G2
NS
T0
T2
T4
T8
C
Asynchronous
Synchronous
T0 T2 T4 T8
Asynchronous
Synchronous
T0 T2 T4 T8
Click - + + + + + - + + + + +
PCNA
MCM7
H3
iPOND
input
D
PCNA
MCM7
H3
Fold increase (T0=1)
T0 T2 T4 T8

Figure 5

A

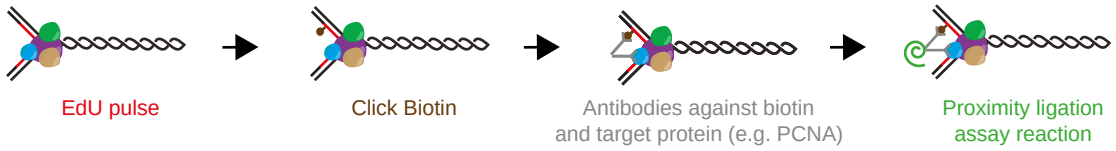
EdU pulse
Click Biotin
Antibodies against biotin
and target protein (e.g. PCNA)
Proximity ligation
assay reaction

B

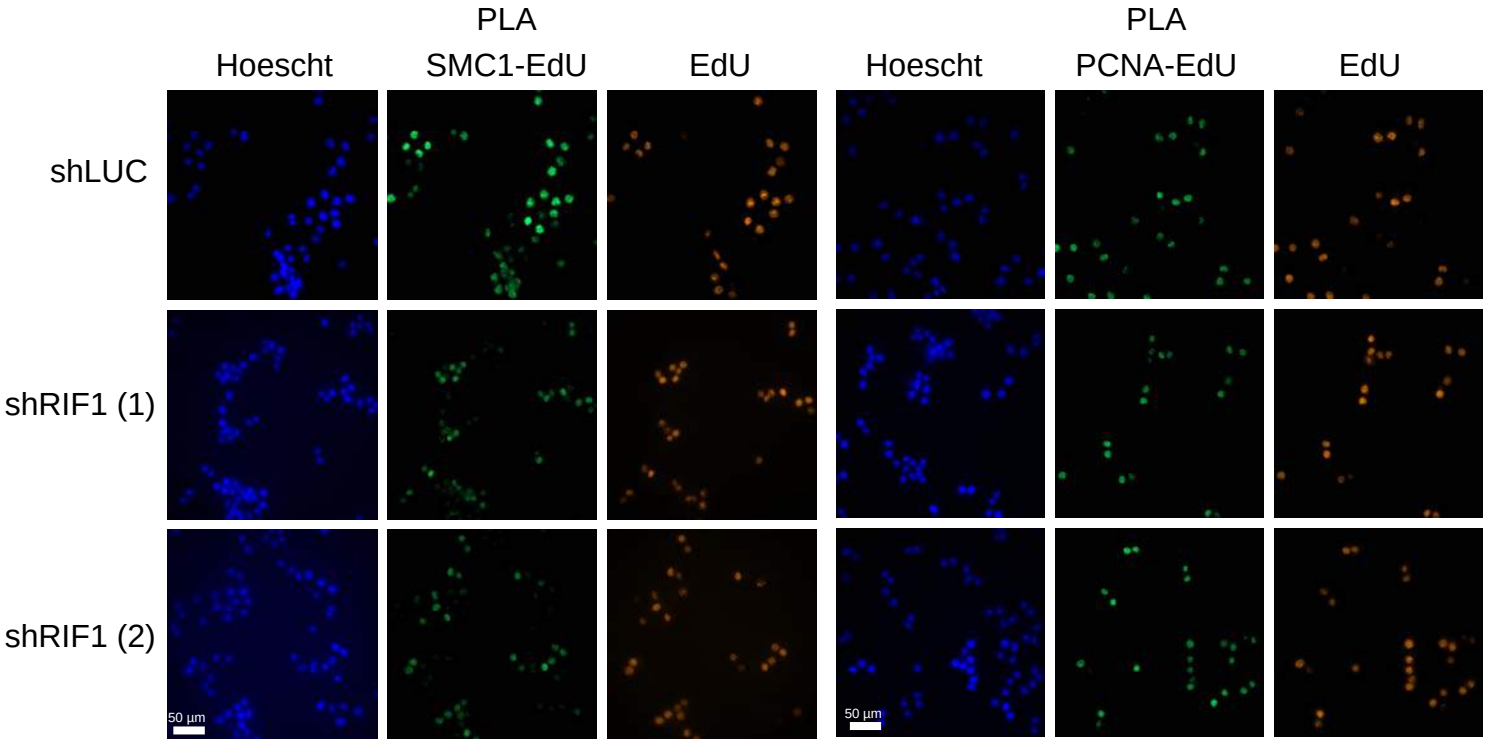
PLA
Hoescht
SMC1-EdU
EdU
PLA
Hoescht
PCNA-EdU
EdU
shLUC
shRIF1 (1)
shRIF1 (2)
50 µm
50 µm

C

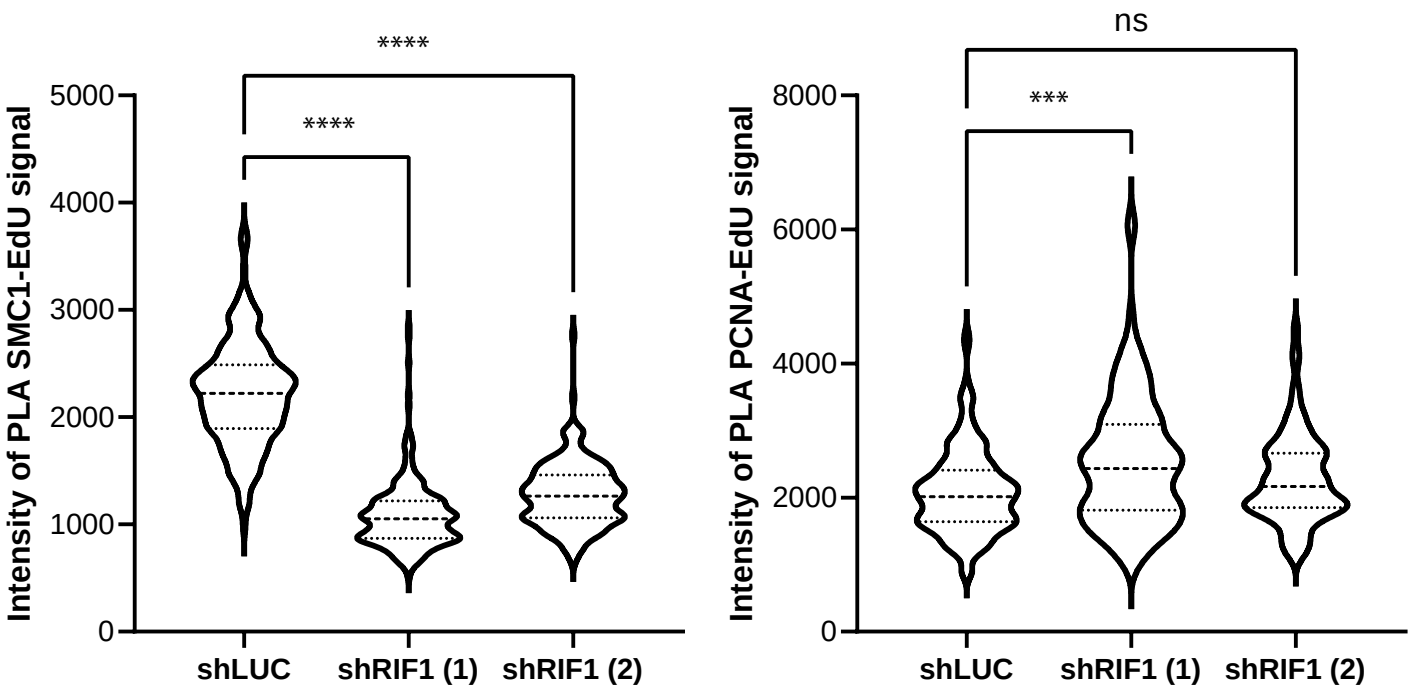
****
****
Intensity of PLA SMC1-EdU signal
5000
4000
3000
2000
1000
0
shLUC
shRIF1 (1)
shRIF1 (2)
ns
***
Intensity of PLA PCNA-EdU signal
8000
6000
4000
2000
0
shLUC
shRIF1 (1)
shRIF1 (2)

Figure 6

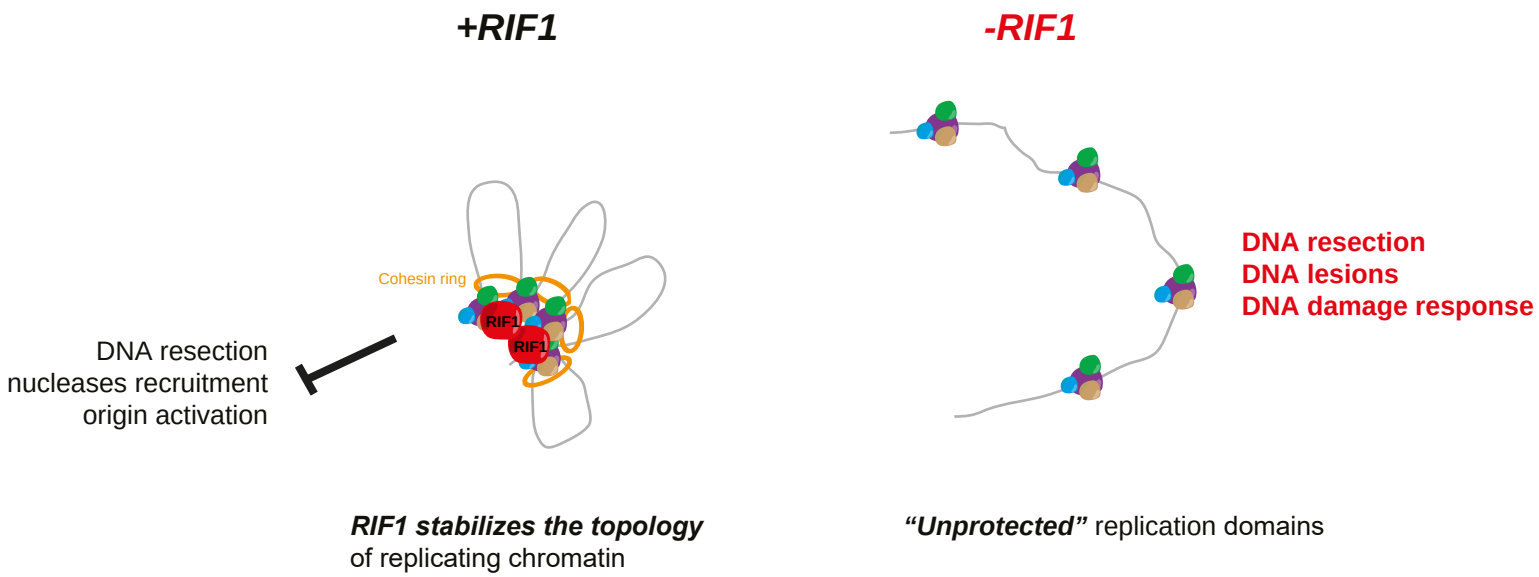
+RIF1
-RIF1
Cohesin ring
RIF1
RIF1
DNA resection
nucleases recruitment
origin activation
DNA resection
DNA lesions
DNA damage response
RIF1 stabilizes the topology
of replicating chromatin
"Unprotected" replication domains

Sup Figure 1

A

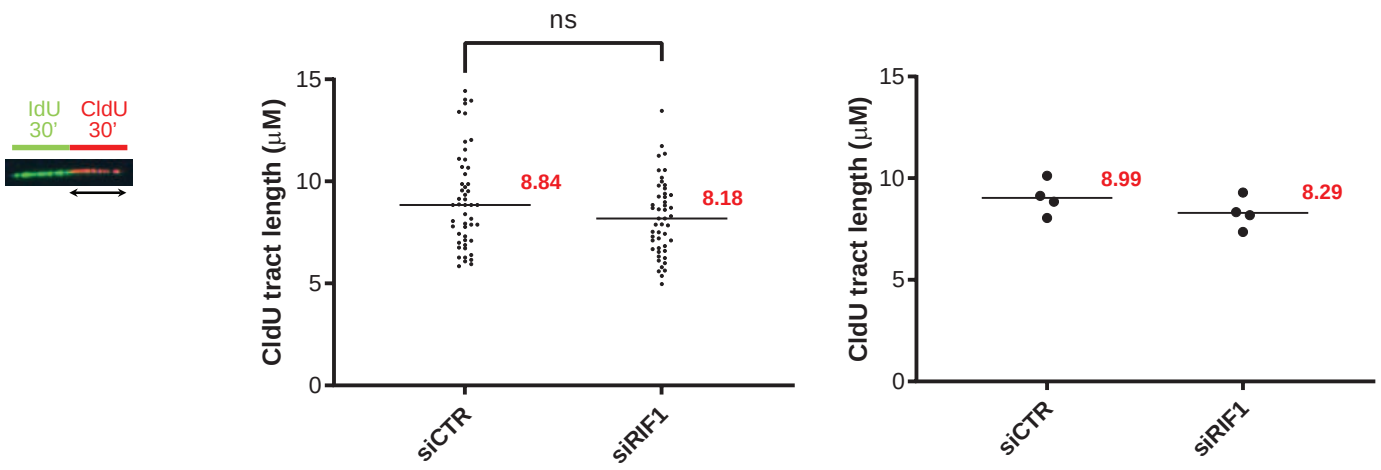

B

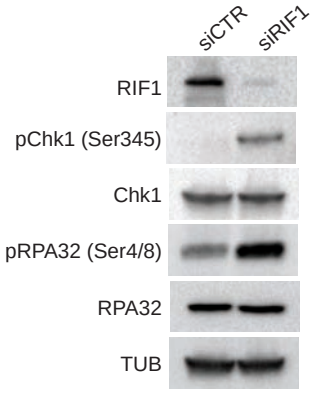

C

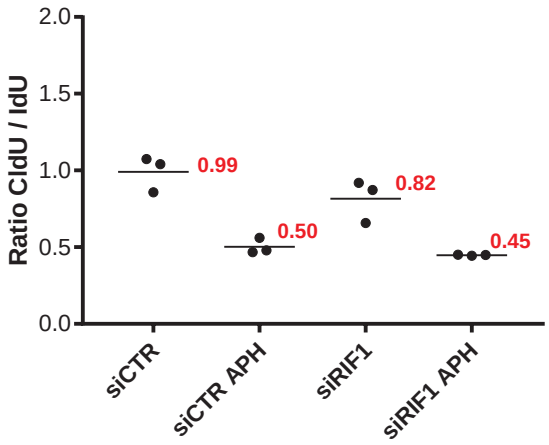

D

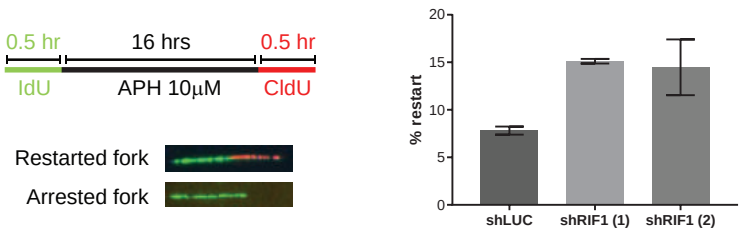

Sup Figure 2

A

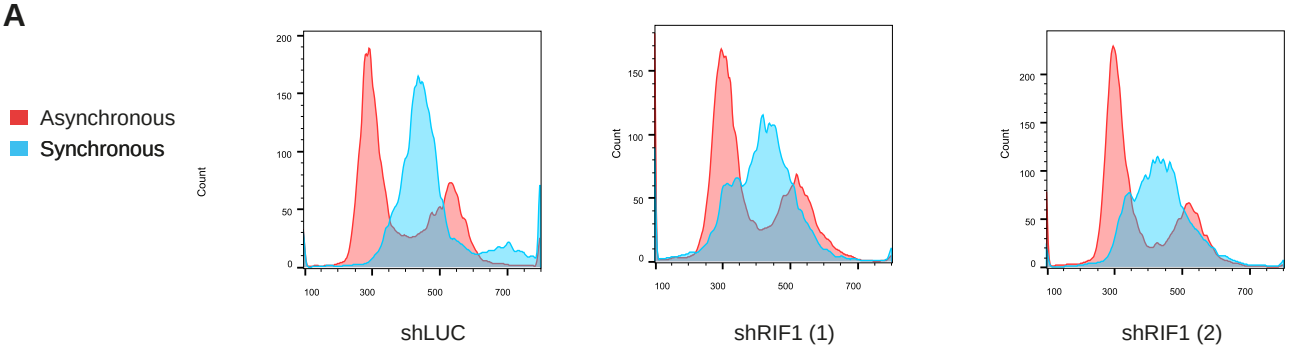

B

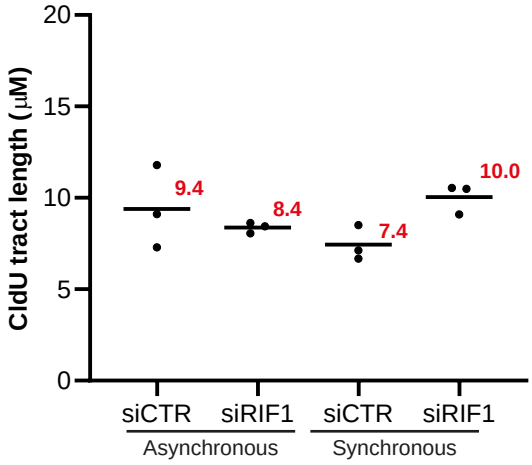

Sup Figure 3

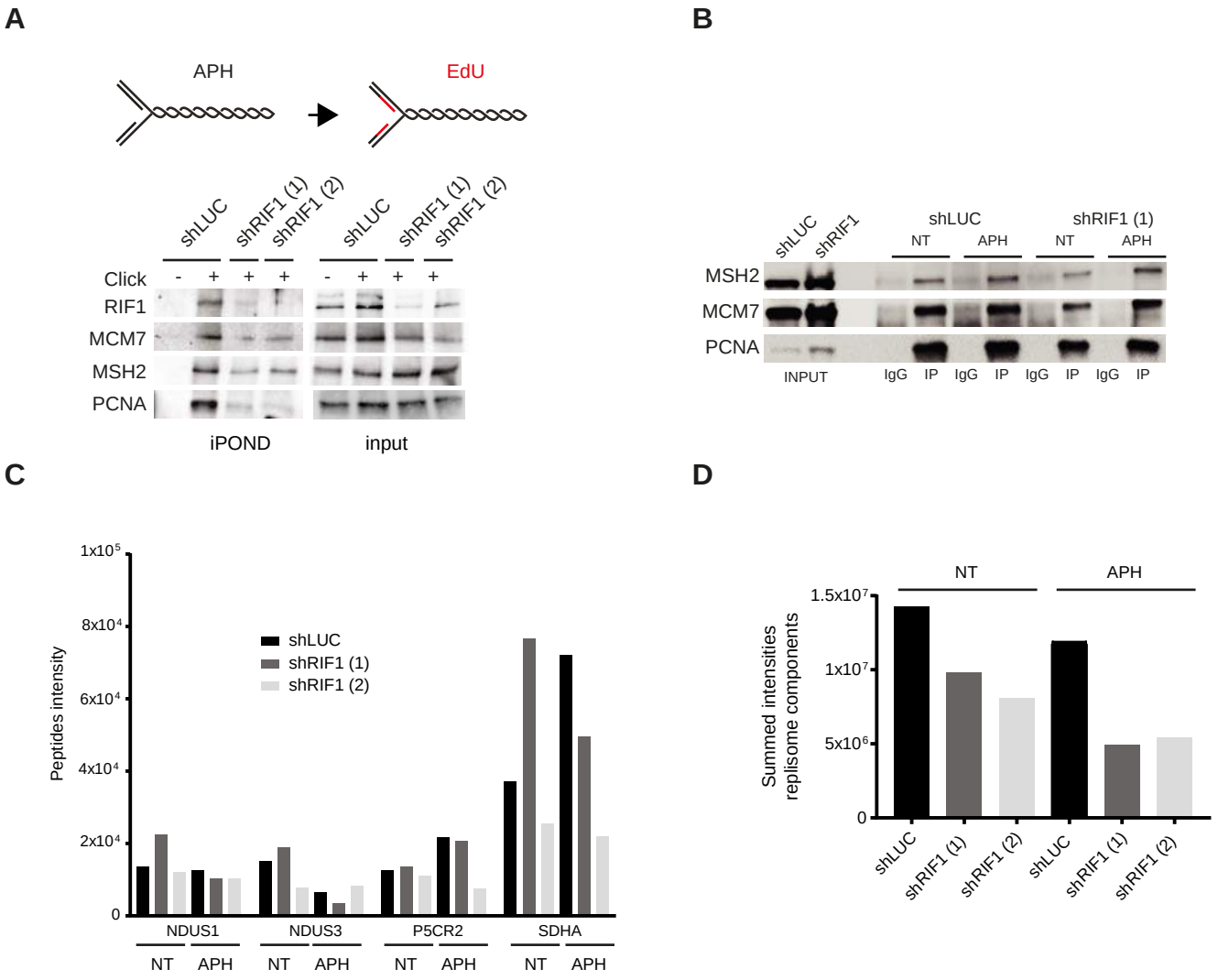
A
APH
EdU
shLUC
shRIF1 (1)
shRIF1 (2)
shLUC
shRIF1 (1)
shRIF1 (2)
Click
- + + +
- + + +
RIF1
MCM7
MSH2
PCNA
iPOND
input
B
shLUC
shRIF1
shLUC
shRIF1 (1)
NT
APH
NT
APH
MSH2
MCM7
PCNA
INPUT
IgG IP IgG IP IgG IP IgG IP
C
Peptides intensity
1x10⁵
8x10⁴
6x10⁴
4x10⁴
2x10⁴
0
shLUC
shRIF1 (1)
shRIF1 (2)
NDUS1
NDUS3
P5CR2
SDHA
NT APH NT APH NT APH NT APH
D
NT
APH
Summed intensities replisome components
1.5x10⁷
1x10⁷
5x10⁶
0
shLUC
shRIF1 (1)
shRIF1 (2)
shLUC
shRIF1 (1)
shRIF1 (2)

Sup Figure 4

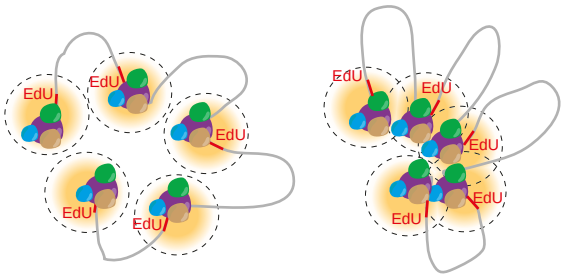

S-phase	***Early/Mid***	***Late***
Clusterization	***Low***	***High***
Probability to capture indirectly replisomes	***Low***	***Strong***

Sup Figure 5

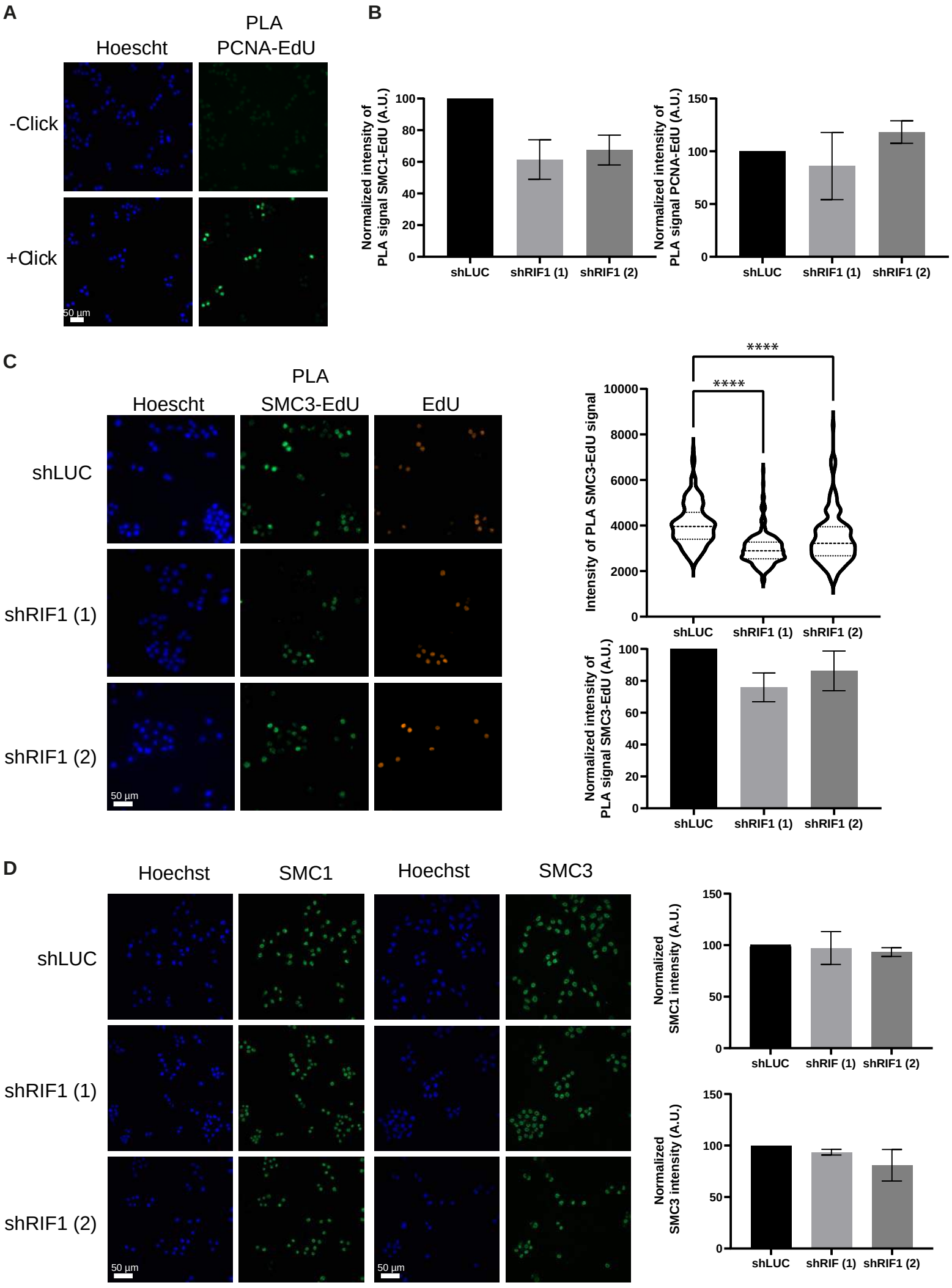
A
PLA
Hoescht
PCNA-EdU
-Click
+Click
50 µm
B
Normalized intensity of PLA signal SMC1-EdU (A.U.)
0
20
40
60
80
100
shLUC
shRIF1 (1)
shRIF1 (2)
Normalized intensity of PLA signal PCNA-EdU (A.U.)
0
50
100
150
shLUC
shRIF1 (1)
shRIF1 (2)
C
PLA
Hoescht
SMC3-EdU
EdU
shLUC
shRIF1 (1)
shRIF1 (2)
50 µm
****
****
Intensity of PLA SMC3-EdU signal
0
2000
4000
6000
8000
10000
shLUC
shRIF1 (1)
shRIF1 (2)
Normalized intensity of PLA signal SMC3-EdU (A.U.)
0
20
40
60
80
100
shLUC
shRIF1 (1)
shRIF1 (2)
D
Hoechst
SMC1
Hoechst
SMC3
shLUC
shRIF1 (1)
shRIF1 (2)
50 µm
50 µm
Normalized SMC1 intensity (A.U.)
0
50
100
150
shLUC
shRIF (1)
shRIF1 (2)
Normalized SMC3 intensity (A.U.)
0
50
100
150
shLUC
shRIF (1)
shRIF1 (2)